INTERNATIONAL ATOMIC ENERGY AGENCY
UNITED NATIONS EDUCATIONAL, SCIENTIFIC AND CULTURAL ORGANIZATION
INTERNATIONAL CENTRE FOR THEORETICAL PHYSICS
I.C.T.P., P.O. BOX 586, 34100 TRIESTE, ITALY, CABLE CENTRATOM TRIESTE

H4-SMR 393/62

SPRING COLLEGE ON PLASMA PHYSICS

15 May - 9 June 1989

TECHNOLOGY OF A SMALL PLASMA FOCUS INCORPORATING SOME EXPERIENCES WITH THE UNU/ICTP PFF

S. Lee

Department of Physics
University of Malaya
Kuala Lumpur 59100
Malaysia

TECHNOLOGY OF A SMALL PLASMA FOCUS
INCORPORATING
SOME EXPERIENCES WITH THE UNU/ICTP PFF

S. LEE

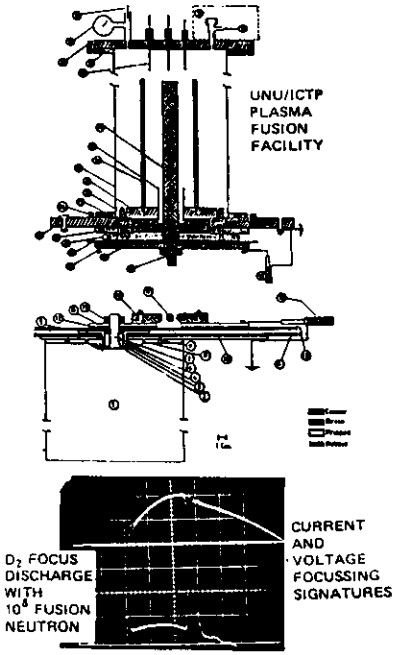

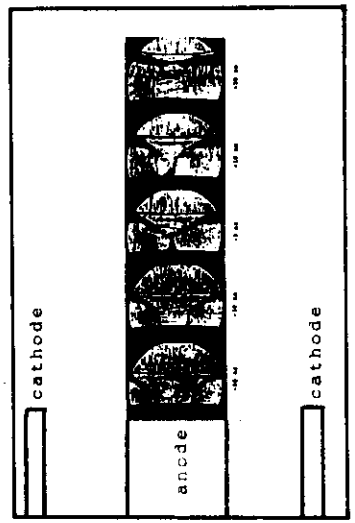

A sequence of Schlieren images showing the plasma structure and dynamics.

Presented at the
Symposium on Small Scale Laboratory Plasma Physics Experiments
(5-7th June 1989)
Spring College on Plasma Physics
(15th May - 9th June 1989)

TECHNOLOGY OF A SMALL PLASMA FOCUS

S. Lee

Plasma/Pulse Research Laboratories
Physics Department/IPT
University of Malaya
59100 Kuala Lumpur, Malaysia

TECHNOLOGY OF A SMALL PLASMA FOCUS

S. Lee

CHAPTER 1

INTRODUCTION

1.1 General Characteristics of the Plasma Focus:

The early work of Filippov[1-3] and Mather [4-6] on the plasma focus has shown that in this device a hot (∿ 1 keV) and dense (∿ 10^{19} cm^{-3}) plasma is created with a lifetime ∿ 50 ns. Considerable interest was directed on this device because of the high nτ value of the plasma and the readily detected bursts of fusion neutrons when operated in deuterium. It has been demonstrated that a capacitor energy of E = 100 J is sufficient to produce a detectable burst of N = 10^5 neutrons. This compares with the 1 MJ Frascati machine on the other end of the scale producing 10^{13} neutrons. A typical machine within the means of a small laboratory may have 10 kJ storage and produces 10^9 neutrons per burst. The yield-energy relationship is simple ($N \sim E^2$) as illustrated by Fig. 1.

Besides being a ready source of hot dense plasma and fusion neutrons (Fig. 2) the focus also emits copious amounts of soft x-ray (Fig. 3). The large range of plasma phenomena readily available from this easily constructed machine has led to its study in many laboratories around the world[7-27].

As a simplification, the focus may be considered as a device which operates in two distinct phases (Fig. 4) an axial acceleration phase in which the characteristics of the device is very similar to an electromagnetic shock tube; and a radial compression phase in which the plasma behaviour may be approximated to a compressing plasma pinch with a length which increases as the radius decreases[28,29,35]. In these two phases the plasma may be considered from the viewpoint of the classical snow-plow model as a well defined plasma slug driven by a magnetic piston (current sheet). These two phases set the stage for the third phase, the short-lived dense plasma phase followed by a fourth phase[30] during which a process of turbulent magnetic

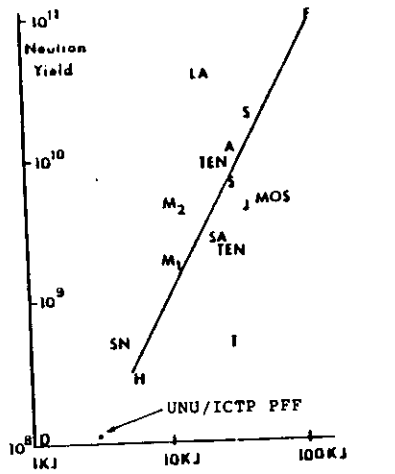

Fig.1 Neutron production as a function of energy.

F=Frascati; LA=Los Alamos; S=Stuggart; A=El Soqunda Aerospace; TEN=Tennessee; MOS=Moscow; J=Julich; SA=Sandia; SN=Steven; T=Texas; M_1=UMDPF1; M_2=UMDPF2; H=Hoboken; D=Darmstadt. (Ref.26, modified)

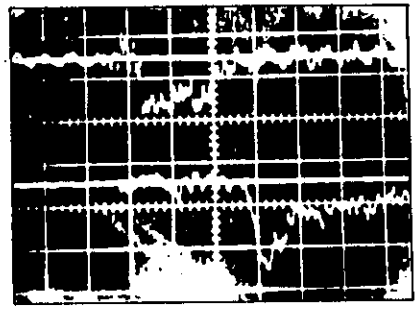

Fig.2 Time-of-flight oscillogram obtained in the measurement of neutron energy. Top trace records output from near detector. Bottom trace records output from far detector placed 10.2 m behind near detector. Horizontal scale 200 ns per cm. (Ref.21)

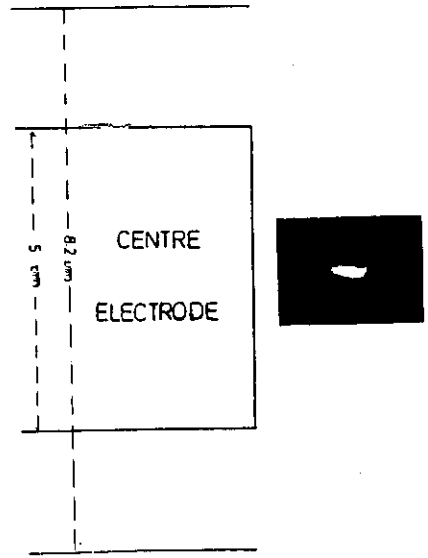

Fig.3 *Soft x-ray photograph in transverse view. The surface of the centre electrode is beyond the left side of the photograph as shown to scale. Voltage, 29.6 kV. Pressure: 1.3 torr. Condenser bank energy 13 kJ.* (REf.41)

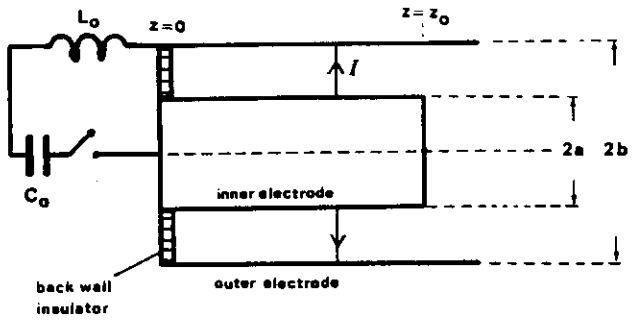

Fig. 4a Phase1: axial acceleration phase

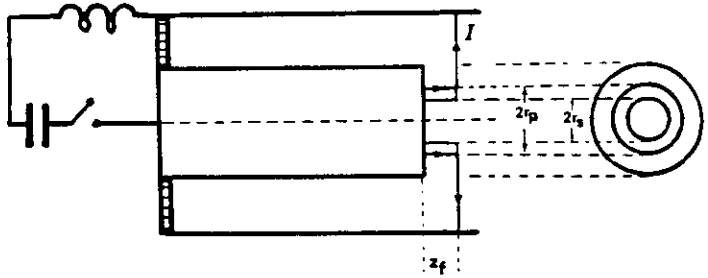

Fig. 4b Phase 2: radial compression phase

(Ref.28)

field penetration[38] results in a quiescent plasma column of relatively large diameter. There is evidence that most of the fusion neutrons are produced during the transition from the third to fourth phase.

1.2 The Device:

The general configuration of the plasm focus device is as shown in Fig. 5.

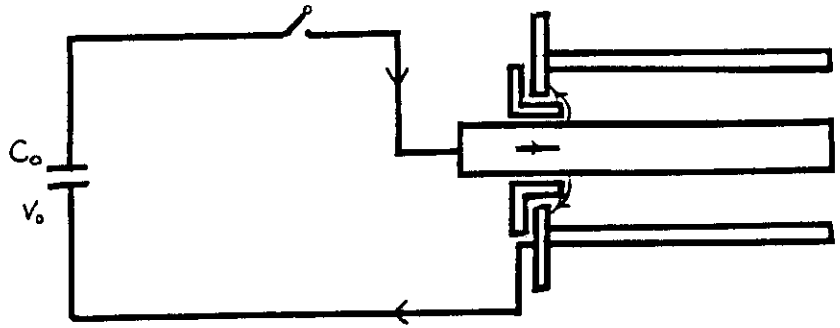

Fig. 5: Schematic of the discharge circuit

1.3 The Phases of Plasma Development:

Break-down and surface discharge:

The device consists of an inner electrode and a coaxial outer electrode separated by an insulator at the starting end. The power source is a capacitor C_o charged to voltage V_o and switched on to the inner electrode by switch S. When S is closed the voltage appears across the two electrodes and when the conditions are properly adjusted a discharge occurs across the surface of the insulator between the inner and outer electrodes. The $\vec{J} \times \vec{B}$ force on this axially symmetric surface current is radially outwards (Fig. 6a). This lifts the current off the insulator in a cylindrical sheet. One end of this sheet remains attached to the inner electrode at the circular junction where the inner electrode meets the insulator. The other end moves radially outwards across the back wall which forms part of the outer electrode.

Axial acceleration phase:

When this lift-off is completed the current flows radially outwards from the inner electrode to the outer electrode in radially symmetric sheet slightly canted in the forward direction (z) at the inner electrode. In this position the $\vec{J} \times \vec{B}$ force on the current sheet is axially down the tube (i.e. in the z direction). The current sheet, scooping up the gas

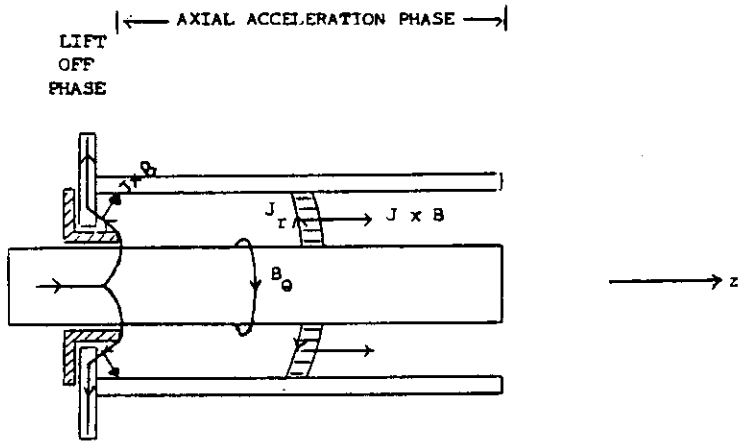

Fig. 6 The driving force in the
a) breakdown region: the JXB force just after breakdown, causing current sheath lift-off.
b) axial acceleration region: the JXB force during the axial phase.

it encounters is thus accelerated down the tube (Fig. 6b). In this phase of axial acceleration the behaviour of the current sheet and the plasma it drives is similar to the situation in an electromagnetic shock tube.

Radial collapse phase:

When the current sheet reaches the end of the centre electrode, the end of the sheet which has been sliding along the centre electrode in the axial direction begins to slide across the face of the centre electrode in the radial inward direction. The other end which has been sliding along the outer electode in the axial direction continues in its motion (Fig. 4b).

Dense plasma phase and focus phase:

In this implosion, a dense plasma column is formed on the axis of the focus tube just off the face of the centre electrode. Towards the end of this dense plasma phase m=0 instabilities set in. The column breaks up and very rapidly a large diameter phase is formed.

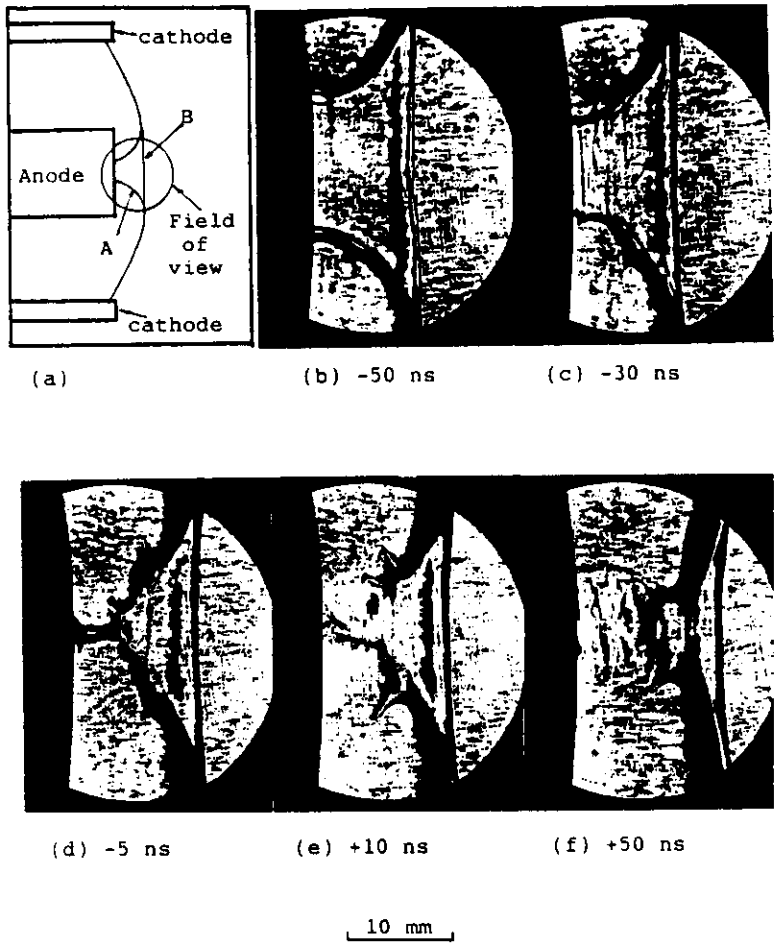

Fig. 7 A sequence of Schlieren images showing the plasma structures and dynamics. Experimental conditions: 9 mbar deuterium at 14 kV. (Ref. 50)

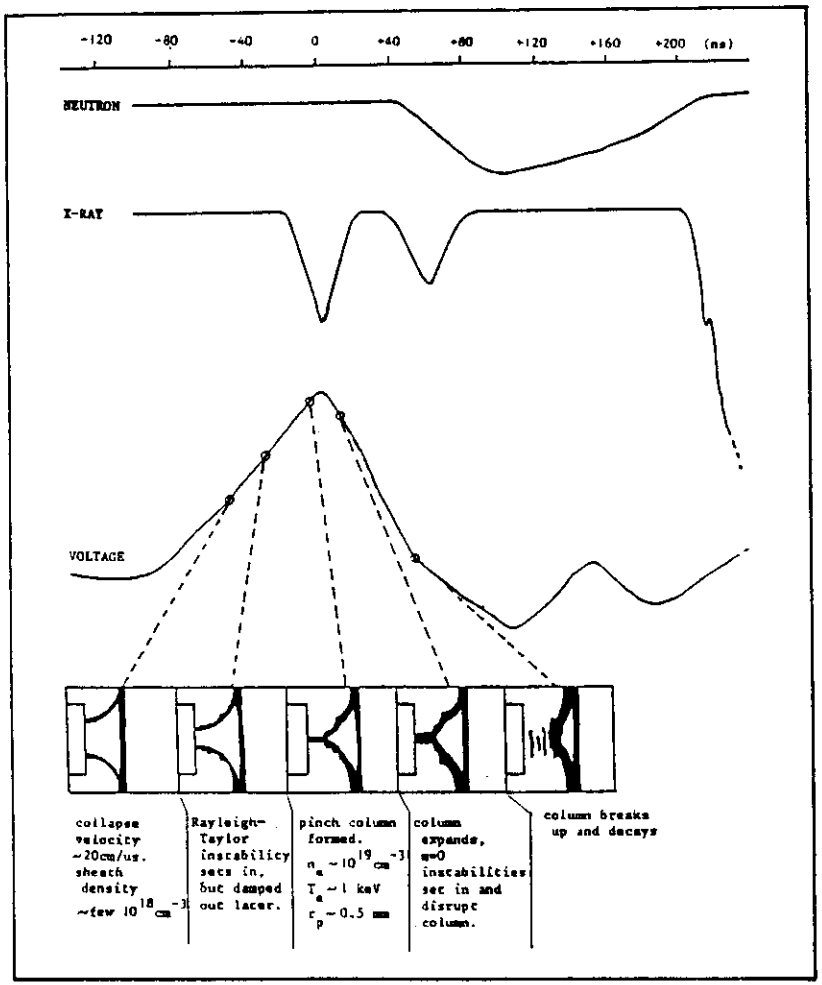

Fig.8 Summary of the temporal development of the radial implosion process (Ref. 50).

The sequence of events from the implosion to the formation of the large diameter plasma has been described in a sequence of framing photographs by Decker and Wienecke[30]. More details of plasma structure giving particularly information on electron density gradient have been obtained by Kwek[49,50] using an entirely Third World home-made Schlieren system including a home-made nitrogen laser light source. This Schlieren sequence (Fig. 7) of radial collapse and subsequent phases are correlated to the measured tube voltage, x-ray and neutron[50] (Fig. 8).

Laser shadowgraphs have also been taken which confirm the main features in the collapse phase and the dense plasma phase (Fig. 9).

Following the dense plasma phase, the column is very rapidly disrupted. This rapid disruption is consistently observed, for example, in the shadowgraphy of Fig. 9 (see the frame at t = + 50 ns). There is also consistent evidence[30] to show that whilst the soft x-ray from the plasma is associated mainly with the dense plasma phase, the hard x-ray is more to be associated with the instability phase and the neutron production peaks between the instability and the expansion phase.

The angular distribution of the neutrons from the plasma focus has been extensively studies (for example, see Fig. 10).

1.4 Classic Indication of Focus Action:

Figure 11 shows the classic indications of strong focussing action (note the severe current dip and the corresponding voltage spike near the middle of the horizontal axis), which in a deuterium focus invariably signals the production of neutrons.

1.5 A Low Cost Device:

The IAEA Consultants' Meeting in Swierk, Poland[45] in December 1978 has recommended the plasma focus as one of the two devices which might be purchased or constructed by a developing country with the intention of studying high temperature plasmas. A figure of likely cost of US$10,000 was mentioned in the Report.

For the purpose envisaged by the Consultants' Report the focus is certainly an eminently suitable machine, as within one low-cost well-behaved machine shock waves, pinch and focus phenomena may be studied: with plasma conditions extending to fusion conditions with copious emission of x-rays and fusion neutrons.

This has been demonstrated in a package designated as the UNU/ICTP PFF (United Nations University/International Centre for Theoretical Physics Plasma Fusion Facility)[51,52] developed for a series of UNU and ICTP sponsored training programmes aimed at initiating experimental plasma research in developing countries. As a result of the training programmes this device with various modifications and improvements is in varying stages of development in Pakistan, Indonesia, India, Egypt, Nigeria, Sierra Leone and Thailand. The training programmes have initiated and assisted in the production of several M.Sc. theses on experimental laser and plasma physics at the Rivers State University of Science and Technology in Nigeria and the UNU/ICTP PFF programme has produced the first Ph.D. in experimental plasma/fusion physics in Pakistan[53].

1.6 Sub-systems of the UNU/ICTP PFF:

For effective initiation of experimental research in developing country experience has shown that the technology/research transfer process is most effectively carried out by the concept of open-box (as opposed to black box) sub-systems. The package is divided into sub-systems (see Fig. 12), each sub-system specifically designed for simplicity, cost-effectiveness and transferability. Each sub-system is then designed and constructed by a trainee and tested to be operational. The sub-systems are then assembled, tested to obtain good and consistent dynamics in various gases and finally to produce a consistent and reproducible neutron yield when operated in deuterium.

The package is then disassembled, packed and airfreighted back to the trainee's home institute, and reassembled and modified for the trainee's own developmental and research purposes.

Since the purposes of this monograph is to describe the technology of a small plasma focus in a manner useful for developing countries it is elected to follow the proven pedagogical approach of the UNU/ICTP PFF. Chapter 2 will describe a simplified dynamic model which enables the focus to be simulated and designed, leading very naturally to computation packages and design criteria, discussed in Chapter 3. Chapter 4 deals with the hard-ware of the UNU/ICTP PFF in sub-system form whilst Chapter 5 describes some possible applications of the plasma focus including some ideas on improving its scaling.

Fig. 9 Side on laser shadowgraph of a 20-kV 60 μF, 4-Torr deuterium plasma focus, showing a pinch ratio $r_p/r_a \sim 0.13$. (Ref. 35,36)

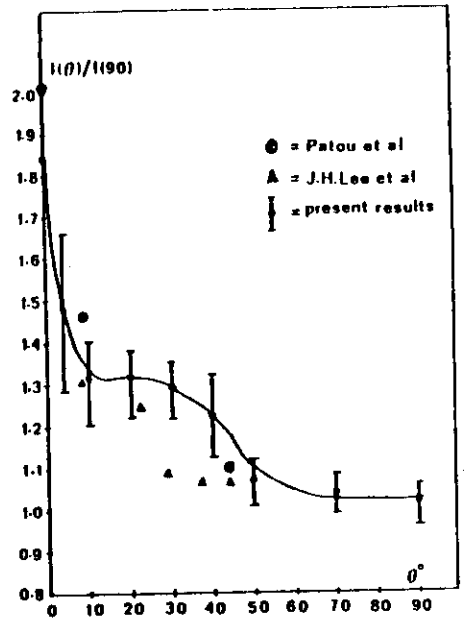

Fig. 10 **Results of angular distribution of neutrons from plasma focus.** (REf.42)

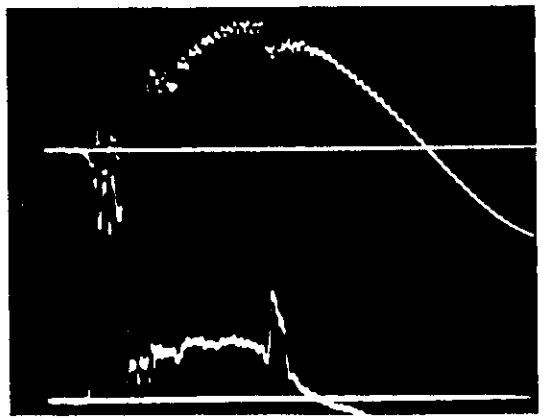

Fig. 11 *Typical current dip and voltage spike of a focusing shot. Top trace: current oscillogram: vertical scale: 200 kA per cm. Bottom trace: voltage oscillogram: vertical scale: 6 kV per cm, horizontal scale: 1 μsec per cm. The characteristic current dip and voltage spike of a good focus are evident at t = 4 μsec.*

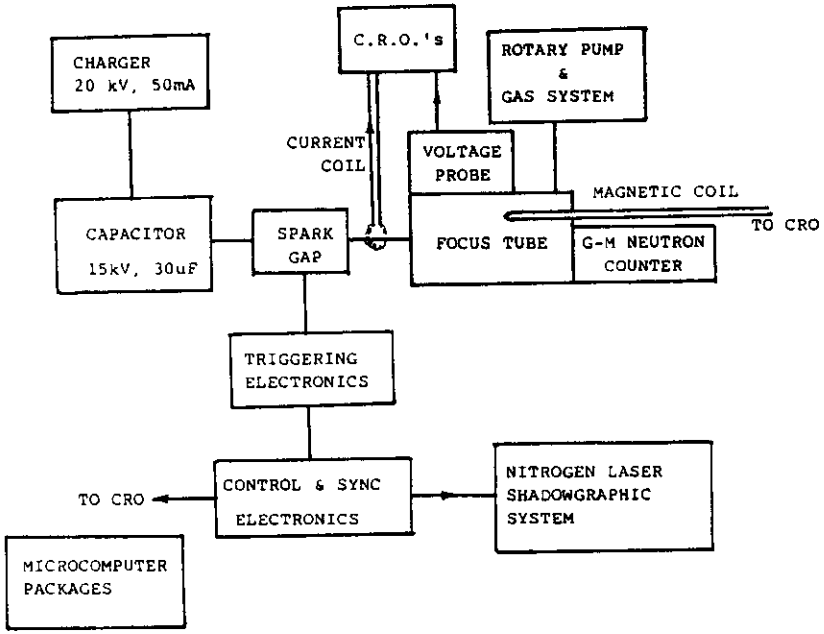

Fig. 12 Sub-systems for the UNU/ICTP PLASMA FUSION FACILITY

CHAPTER 2

DYNAMIC THEORY OF THE PLASMA FOCUS

2.1 Review:

The plasma focus is now well established as a device by which a hot, dense plasma may be produced with consequent generation of fusion neutrons. The key technical and experimental features of this device are now well documented so that a simple functional device may be built without resorting to sophisticated technology. The situation concerning the theoretical treatment of the device is however quite different. The axial acceleration region poses no problem, but there has been no simple method of computing even the dynamics of the radial pinching phase. Potter[44] has set up a two-dimensional code which gives a detailed description of the axial acceleration phase as well as the radial pinching phase, However the code is complex and its accuracy during the axial acceleration phase had to be checked against the predictions of a simple one-dimensional snow-plow model. The radial implosion phase could not be checked against a simple physical model because none existed which could give even a physically acceptable quasi-equilibrium radius. Recently, Zakaullah[33] has developed a two-dimensional model with scaling parameters suitable for device design.

Simple physical models have been constructed for the plasma focus based on the snow-plow equation. As is well known this model when applied to a radial compression gives a zero-radius column. Attempts have been made to overcome this by devising a retarding kinetic pressure term. Other attempts use criteria for the minimum radius such as the Larmor radius. However Lee[29] has shown that these methods are not energy-consistent and therefore should be replaced by an energy-balance model which provides the correct end-point for the implosion trajectory, thus giving the correct quasi-equilibrium radius. Combining the conventional snow-plow model with an energy-balance criterion enables a complete energy-consistent trajectory to be obtained[43].

The snow-plow model however is essentially a structureless model. Potter[34] has suggested a slug model which he has applied to the specific case of a constant current, constant length pinch to obtain a collapsing layer with structure. We extend this slug model to the radial compression phase of the plasma focus, allowing the length of the pinching column and the plasma current to vary self-consistently.

2.2 The Plasma Focus Dynamics:

We shall consider two distinct phases of the plasma focus dynamics (a) the axial phase and (b) the radial pinch phase.

Figure 4 illustrates the two phases of the focus dynamics.

In this model when the capacitor at voltage V_o is switched onto the focus tube breakdown first occurs across the back-wall insulator. A current sheath is formed axisymmetrically. It lifts off from the backwall and is then propelled by its own $J_r B_\theta$ force down the annular channel in the z-direction. When the current sheath comes to the position $z = z_o$ the radial phase starts. The radial pinch proceeds as shown in Fig. 4b.

For the axial phase, we shall consider a snow-plow model in which when the current sheath is at position z, all its accumulated mass is also at position z. This is an approximation which does not give rise to any fundamental problem in the axial phase.

In the radial phase, however, if this 'thin' snow-plow model is used it will give rise to a compression to zero radius unless the compression is correctly terminated by an energy balance principle. However, if a slug-model (with structure) is used, a shock front will separate out from the current sheath (magnetic piston) and a finite thickness plasma layer will result. This layer will be propelled radially inwards by the $J_z B_\theta$ force. As the plasma layer collapses inwards the whole column elongates (since the compression is open-ended at one end). In the slug-model when the shock hits the axis, the piston stops and a quasi-equilibrium is formed. However, a check with energy balance indicates that the piston will continue to move a little so that the final quasi-equilibrium radius should be determined by energy balance.

It is well known that the majority of neutrons are produced in the break-up phase following the radial quasi-equilibrium described above. However no theory yet exists to explain this break-up phase; and we shall hence confine ourselves to the relatively well-ordered description of the dynamics of the axial and radial pinch phase; in the hope that an understanding of these phases could eventually lead to greater understanding of the final break-up phase.

The Axial Phase - Snow-plow Model:

The Equation of Motion

In the axial phase, consider that the current sheath scoops up (snow-plows) all the mass it encounters. Thus at a position z, the mass entrained by the sheath is:

$$\rho_o\{\pi(b^2 - a^2)z\} \ ;$$

and the rate of change of momentum of the sheath is:

$$\text{motion:} \qquad \frac{d}{dt}\{\pi\rho_o(b^2 - a^2)z\,\frac{dz}{dt}\} = \frac{\mu I^2}{4\pi}\,\ell n\frac{b}{a} \qquad (1)$$

where the right hand side is the force exerted by the self-magnetic field ($B = \mu I/2\pi r$) of the current sheath integrated over the whole current sheath between r=b to r=a. In this equation z and I, the circuit current, are in general functions of time. To determine the current I, the circuit equation is needed.

The Circuit Equation

The equivalent circuit of the focus tube is presented schematically below.

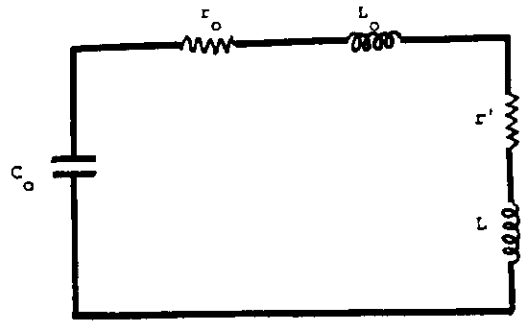

Equivalent circuit of plasma focus tube

Here C_o, L_o, r_o are the fixed capacitance, inductance and resistance of the external elements and r' and L are the plasma resistance and inductance respectively. Assume that r_o and r' are negligibly small, we may use Kirchhoff's second law to write the voltage equation for the

circuit. Thus:

$$\text{Circuit:} \qquad \frac{d}{dt}\{(L_o + L)I\} = V_o - \frac{\int_o^t I dt}{C_o} \tag{2}$$

where the plasma inductance may be written as a function of z:

$$L = \frac{\mu}{2\pi} \ell n \frac{b}{a} z \tag{3}$$

Equation (3) thus may be written as:

$$\text{Circuit:} \qquad \frac{dI}{dt} = \frac{V_o - \frac{\int I dt}{C_o} - \frac{\mu}{2\pi} \ell n \frac{b}{a} I \frac{dz}{dt}}{\{L_o + \frac{\mu}{2\pi} \ell n \frac{b}{a} z\}} \tag{4}$$

Equations (1) and (4) are the two equations determining the behaviour of z and I.

Normalization

Equations (1) and (4) may be written in normalized form for the following purpose:

a) To simplify the system of equations so that its basic functional dependance may be seem more clearly,

b) To introduce scaling parameters which enable all ranges of operation of the shock tube to be covered simply by a variation of the scaling parameters. The identification of the correct scaling parameters is equivalent to identifying the ratios which govern the regimes of operation of the shock tube.

For the axial phase of the plasma focus there are two relevant ratios:

i) the ratio of the capacitor discharge time to the transit time of the sheath from z=0 to z=z_o.

ii) the ratio of L_o to the maximum tube axial inductance.

c) To obtain an expression for the characteristic transit time, which is derived naturally in the process of normalization.

The first step in normalization is to choose the correct reference quantities to normalize the variables. Here we take:

$$\zeta = \frac{z}{z_o}, \qquad \tau = \frac{t}{t_o}, \qquad \imath = \frac{I}{I_o}$$

where z_o = length of the axial phase,

$t_o = \sqrt{(L_o C_o)}$, the angular frequency of the L_o-C_o circuit (the short-circuited capacitor bank),

and $I_o = V_o/\sqrt{(L_o/C_o)}$, the peak current of the L_o-C_o circuit.

With this normalization, the equation of motion (1) becomes:

$$\text{motion:} \qquad \frac{d^2\zeta}{d\tau^2} = \frac{\alpha^2 \imath^2 - (\frac{d\zeta}{d\tau})^2}{\zeta} \tag{5}$$

where the first scaling parameter is introduced as a ratio of the two characteristic times t_o and t_a:

$$\alpha = \frac{t_o}{t_a}$$

and t_a appears naturally as a characteristic axial transit time defined as:

$$t_a = \{\frac{4\pi^2(b^2 - a^2)}{\mu \ell n \frac{b}{a}}\}^{\frac{1}{4}} \frac{z_o \rho_o^{\frac{1}{2}}}{I_o} \tag{6}$$

Similarly, the circuit equation becomes:

$$\text{circuit:} \qquad \frac{d\imath}{d\tau} = \frac{1 - \int \imath d\tau - \beta \imath \frac{d\zeta}{d\tau}}{1 + \beta\zeta} \tag{7}$$

where the second scaling parameter is seen to be a ratio of two inductances:

$$\beta = \frac{\frac{\mu}{2\pi} \ell n \frac{b}{a} z_o}{L_o}$$

Equations (5) and (7) may be integrated to give the solution of $\imath$ and ζ.

Initialization

The initial conditions are:

$$\tau = 0, \quad \zeta = 0, \quad \frac{d\zeta}{d\tau} = 0, \quad \frac{d^2\zeta}{d\tau^2} = \sqrt{(\frac{\alpha^2}{3})}, \quad \imath = 0$$

$$\frac{d\imath}{d\tau} = 1 \quad \text{and} \quad \int \imath d\tau = 0$$

Integration

Equations (5) and (7) may now be integrated for any selected

values of α and β. Even a linear method such an Euler's give sufficient accuracy with time step of $\Delta\tau = 0.001$.

The integrations stops at $z = z_o$.

The Radial Compression Phase:

Radial Shock Motion

Figure 4b shows the geometry of the compressing column. At a given time t the magnetic piston has moved to the position r_p from 'a' driving a shock front ahead of it at position r_s. All the gas encountered by the shock front in its journey from 'a' to r_s is now contained between r_s and r_p. This forms a 'slug' of plasma. Because of the diverging streamlines through the region bounded by r_s and r_p conditions through the slug are in general functions of r and may not be considered to be uniform from one value of r to another at any given time t. However because the shock-front is assumed to be thin the planar shock-jump equations hold across the shock front.

In the radial phase the magnetic piston is knwon to be highly supersonic and therefore the sound speed in the slug is large compared to the particle speed. Under these conditions we may make the assumption that the one quantity that may be taken as uniform across the slug is the pressure P. Thus this pressure P may be related by the shock-jump equations to the shock speed $v_s = dr_s/dt$ as: (see Ch. VI Sec. 2.12 of this Volume)

$$P = \frac{2}{\gamma + 1} \rho_o v_s^2 \tag{8}$$

Further, at the magnetic piston we may equate the pressure P to the magnetic pressure P_B so that: (see Ch. VI Sec. 2.9 of this Volume)

$$P = P_B \tag{9}$$

where
$$P_B = \frac{\mu I^2}{8\pi^2 r_p^2} \tag{10}$$

Thus from Eqns. (8) to (10) we have:

radial shock motion
$$v_s = \frac{dr_s}{dt} = -\left\{\frac{\mu(\gamma+1)}{\rho_o}\right\}^{\frac{1}{2}} \times \frac{I}{4\pi r_p} \tag{11}$$

where the negative sign indicates radial inward motion.

Axial Shock Motion

Since the compression is open at one end we expect an axial shock to be propagated in the z-direction. Further we may assume that the pressure driving the radial shock is the same as that driving the axial shock. Thus, the length of the radial compression z_f increases during the compression and this is one of the major factors responible for the high compressions in the plasma focus. We may write

Axial shock motion:
$$\frac{dz_f}{dt} = -\frac{dr_s}{dt} \tag{12}$$

The Circuit Equation

The circuit equation for the system in the pinch phase may be written in the same manner as in Eqn. (2); but we note that now:

$$L = \frac{\mu}{2\pi}\left(\ell n \frac{b}{a}\right) z_o + \frac{\mu}{2\pi}\left(\ell n \frac{b}{r_p}\right) z_f \tag{13}$$

where both z_f and r_p vary. Thus the circuit equation may be written as:

circuit equation
$$\left\{L_o + \frac{\mu}{2\pi}\left(\ell n \frac{b}{a}\right) z_o + \frac{\mu}{2\pi}\left(\ell n \frac{b}{r_p}\right) z_f\right\} \frac{dI}{dt}$$
$$+ I\frac{\mu}{2\pi}\left(\ell n \frac{b}{r_p}\right)\frac{dz_f}{dt} - I\frac{\mu}{2\pi}\frac{z_f}{r_p}\frac{dr_p}{dt} = V_o - \frac{\int I dt}{C_o} \tag{14}$$

Radial Piston Motion

Equations (11), (12) and (14) are insufficient to define the problem since there are four variables r_s, r_p, z_f and I to be determined as functions of time. The fourth equation may be obtained by applying the adiabatic expansion law to a fixed mass of gas in the slug at any given instant. For this we write:

$$PV^\gamma = \text{constant} \tag{15}$$

$$\text{or} \quad \frac{\gamma dV}{V} + \frac{dP}{P} = 0 \tag{16}$$

where γ is the effective specific heat ratio of the plasma and the volume of the slug is:

$$V = \pi(r_p^2 - r_s^2) z_f \tag{17}$$

To eliminate V from Eqn. (16) we need to differentiate Eqn. (17) to obtain dV as a function of dr_p, dr_s and dz_f. To do this we need to

consider very carefully so that the differential quantities dr_p, dr_s and dz_f are applied to a fixed mass of gas. For example when the piston moves by dr_p no new mass of gas is introduced into the corresponding new volume V + dV. However when the shock front moves from r_s to $r_s + dr_s$ it admits into the new volume V + dV a new mass of gas. This new mass of gas is compressed by a ratio $(\gamma+1)/(\gamma-1)$ and will occupy part of the increase in volume, so that the actual increase in volume available to the original mass of gas in volume V does not correspond to the increment dr_s but to an effective (reduced) increment $dr_s x 2/(\gamma+1)$. This also applies to the increment dz_f.

Thus to apply the adiabatic law of Eqn. (16) to the slug we need to write the differential of Eqn. (17) in the following form:

$$dV = 2\pi(r_p dr_p - \frac{2}{\gamma+1} r_s dr_s) z_f + (r_p^2 - r_s^2)\frac{2\pi}{\gamma+1} dz_f \qquad (18)$$

giving us:

$$\frac{dV}{V} = \frac{2(r_p dr_p - \frac{2}{\gamma+1} r_s dr_s) z_f + (r_p^2 - r_s^2)\frac{2}{\gamma+1} dz_f}{z_f(r_p^2 - r_s^2)} \qquad (19)$$

We may also eliminate dP/P from Eqn. (16) by writing from Eqn. (8) and Eqn. (11):

$$\frac{dP}{P} = \frac{2dv_s}{v_s} = 2\left(\frac{dI}{I} - \frac{dr_p}{r_p}\right) \qquad (20)$$

Substituting Eqns. (19) and (20) into Eqn. (16) and rearranging we obtain the adiabatic law in the following form:

Radial piston motion

$$\frac{dr_p}{dt} = \frac{\frac{2}{\gamma+1}\frac{r_s}{r_p}\frac{dr_s}{dt} - \frac{r_p}{\gamma I}\left(1 - \frac{r_s^2}{r_p^2}\right)\frac{dI}{dt} - \frac{1}{\gamma+1}\frac{r_p}{z_f}\left(1 - \frac{r_s^2}{r_p^2}\right)\frac{dz_f}{dt}}{(\gamma-1)/\gamma + (1/\gamma)\, r_s^2/r_p^2} \qquad (21)$$

Normalization

The four equations (11), (12), (14) and (21) form a close set of equations which may be integrated for r_s, r_p, z_f and I. For this phase the following nomalization procedure is adopted:

$\tau = t/t_c$, $\quad \iota = I/I_o$ as in the axial phase but with

$\kappa_p = r_p/a$, $\quad \kappa_s = r_s/a$ and $\quad \zeta_f = z_f/a$.

This gives us, after re-arrangement, the set of equations representing the generalized slug model in normalized form as follows:

Radial shock

$$\frac{d\kappa_s}{d\tau} = -\alpha\alpha_1 \iota/\kappa_p \qquad (22)$$

Axial shock

$$\frac{d\zeta_f}{d\tau} = -\frac{d\kappa_s}{d\tau} \qquad (23)$$

Radial piston

$$\frac{d\kappa_p}{d\tau} = \frac{\frac{2}{\gamma+1}\frac{\kappa_s}{\kappa_p}\frac{d\kappa_s}{d\tau} - \frac{\kappa_p}{\gamma\iota}\left(1 - \frac{\kappa_s^2}{\kappa_p^2}\right)\frac{d\iota}{d\tau} - \frac{1}{\gamma+1}\frac{\kappa_p}{\zeta_f}\left(1 - \frac{\kappa_s^2}{\kappa_p^2}\right)\frac{d\zeta_f}{d\tau}}{(\gamma-1)/\gamma + (1/\gamma)\,(\kappa_s^2/\kappa_p^2)} \qquad (24)$$

Current

$$\frac{d\iota}{d\tau} = \frac{1 - \int \iota d\tau + \frac{\beta_1}{F}(\ell n \kappa_p/c)\iota\frac{d\zeta_f}{d\tau} + \frac{\iota\beta_1}{F}\frac{\zeta_f}{\kappa_p}\frac{d\kappa_p}{d\tau}}{\{1 + \beta - (\beta_1/F)(\ell n \kappa_p/c)\zeta_f\}} \qquad (25)$$

where $c = b/a$ and $F = z_o/a$. The new scaling parameters introduced for the pinch phase are:

$$\alpha_1 = \{(\gamma+1)(c^2-1)\}^{\frac{1}{2}}\, F/(2\ell nc) \text{ and } \beta_1 = \beta/\ell nc.$$

Thus whereas the scaling factors α and β enable the axial phase to be scaled for ratios of capacitor to axial run-down times and axial phase inductance to external inductance, the scaling factors $\alpha\alpha_1$ and β_1 allow the radial phase to be scaled for ratios of capacitor to radial pinch times and for characteristic pinch to external inductances.

The radial phase starts after the axial phase reaches $\tau = \tau_a$ at which time: $\zeta = 1$, $\quad \iota = \iota_a$, $\quad \kappa_s = 1$, $\quad \kappa_p = 1$, and $\quad \zeta_f = 0$.

The radial phase ends when $\kappa_s = 0$ at which time the shock front has reached the axis and the position of κ_p represents κ_m the radius of the quasi-equilibrium column for the pinch phase of the plasma focus.

2.3 Integration:

The integration of Eqns. (5) and (7) and subsequently Eqns. (22)

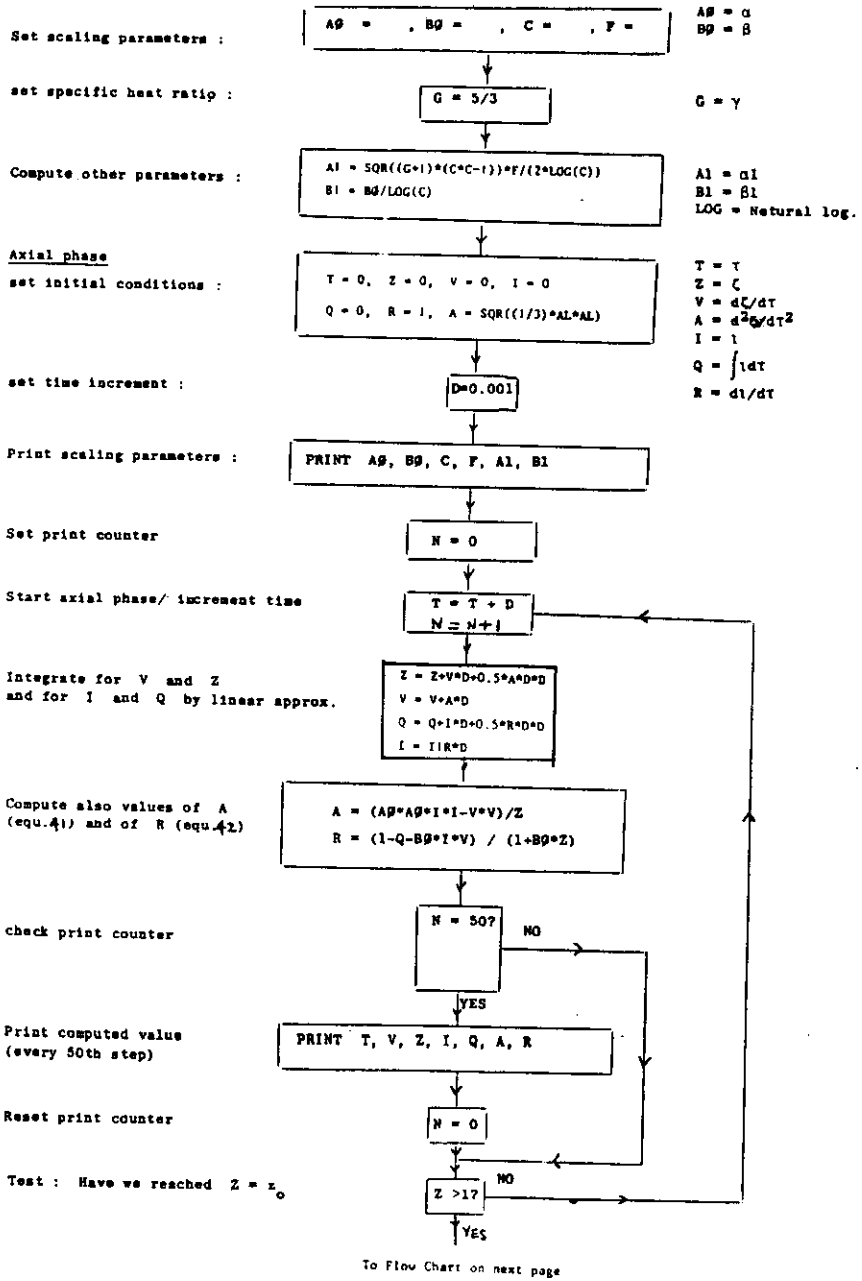

Fig. 13 Flow Chart of Plasma Dynamics Computation of Plasma Focus

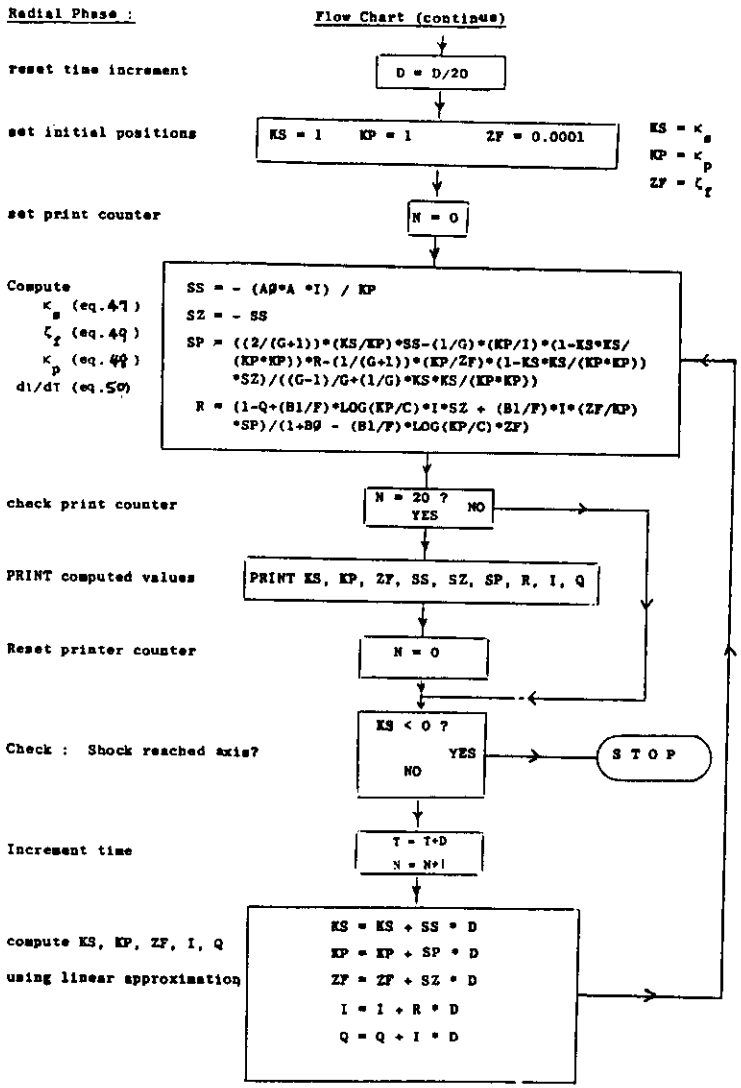

Fig. 13 (continued)

to (25) has been performed using a simple linear approximation method which was checked against a Runge-Kutta method and found to be of sufficient accuracy when 1000 time-steps were taken in each phase[56]. The program runs well in the BASIC language. The flow chart is shown in Fig. 13.

2.4 Results and Discussion:

A typical set of results is shown in Figs. 10a and 10b. Figure 10a shows the trajectory ζ versus τ in the axial phase and the current waveform ι versus τ for both phases. It is seen that already in the axial phase the current has flattened out and reaches a peak value of $0.6I_o$ at around $\tau=1.2$. The slight but clearly noticeable dip in the current just past $\tau = 1.6$ corresponds to the radial collapse phase. The trajectories of this phase κ_p and κ_s versus τ are shown in Fig. 10b on expanded time-scale. For the condition of: $a=1.5$, $\beta=1.0$, $F=6.4$, $\gamma=5/3$ and $c=3.4$ it was found that the quasi-equilibrium radius ratio of the plasma focus pinch is 0.16.

This model presents a relatively simple way for computing the plasma focus trajectory with a quasi-equilibrium radius ratio. The simplicity and low computing requirements of the model makes it very useful for design and optimization studies. The coupling mechanism between the plasma and the magnetic field has been assumed to be purely electromagnetic and this limits the accuracy of the model towards the end of the trajectory as the quasi-equilibrium column is being formed. This is because towards the end of the pinch phase the electron Hall parameter attains values greater than unity and the plasma may become anomalously resistive. This effect, not included in the present dynamic model probably plays a dominant role in the experimentally observed complex structure and dynamics of the actual plasma focus in its phases subsequent to the pinch phase we have discussed.

2.5 Energy Balance Theory for the Quasi-Equilibrium Radius Ratio:

Is the end point of the slug model consistent with energy balance?

For a fast radial compression with no losses it has been found[24,35,43] that the quasi-equilibrium radius is defined from a consideration of energy and pressure balance. These balance conditions give the following

$$\iota_m^2 = \frac{2(\gamma-1)}{f_{rs}\ell_m}\int_{\kappa_m}^{1}\frac{\iota^2\ell d\kappa}{\kappa} \qquad (26)$$

where f_{rs} = reflected shock overpressure,

ι_m = normalized current at the time quasi-equilibrium is reached,

ℓ_m = length of the compressed column at quasi-equilibrium,

and κ_m = radius ratio at quasi-equilibrium.

As an approximation to solve this integral we may assume that during the radial phase ι = constant and $\ell = a-r$ (as indicated by the slug model). Then for $\gamma = 5/3$ and $f_{rs} = \gamma$, the energy balance condition of Eqn. (21) gives

$$\kappa_m = 0.15 .$$

Thus the energy balance theory predicts that the radius of the focus pinch column is reduced further from 0.16 (pinch ratio when shock hits axis according to slug model) to a final value of 0.15. The approximate values of the pinch focus ratios and the further compression (after the shock goes on-axis) have been observed in streak photographs for both deuterium and argon plasma focus[46], and in recent x-ray photographs[47].

Recent observations have shown that when the shock front hits the axis the piston continues to move as though "it were not aware that the shock front had hit the axis". This is of course as expected since the information that the shock front had hit the axis is only communicated to the piston at the local small disturbance speed. The local small disturbances created by the shock front hitting the axis propagates radially outwards in coalescence as the reflected shock wave so that the piston is only aware of these events when hit by the reflected shock front. This is, of course, in variance with the slug model; the breakdown of the model in this region being due to the importance of the fact that the small disturbance speed is not infinite. A simple and may be effective empirical method to complete the solution may be simply to decouple the piston, as suggested by the experimental observations, letting it move in freely until it hits the reflected shock. The trajectory of the reflected shock may be estimated from Guderley's paper[55].

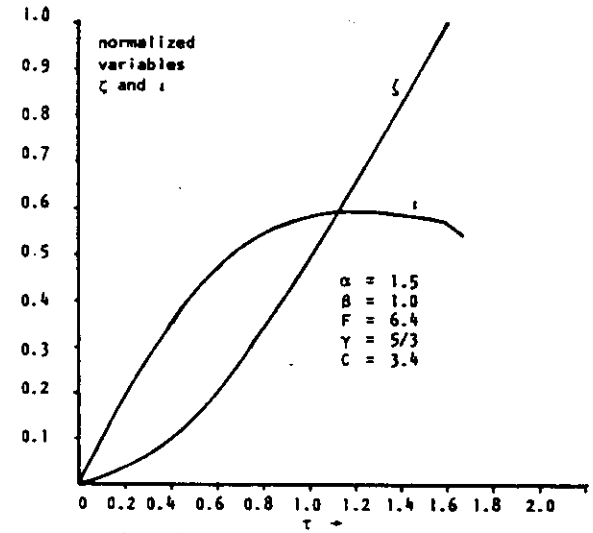

Fig. 14a Solutions of ζ and ι as functions of τ-axial phase

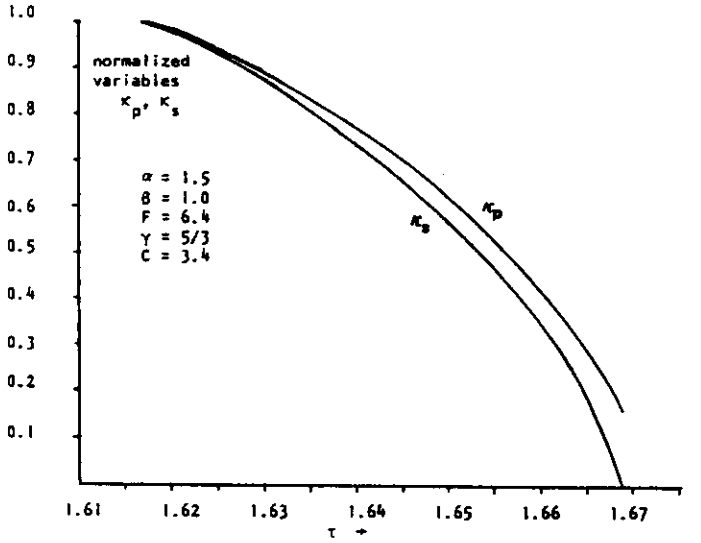

Fig. 14b Solutions of κ_p and κ_s as functions of τ - radial phase

CHAPTER 3

DESIGN OF THE PLASMA FOCUS EXPERIMENT

3.1 Cost Effective Physics:

In order to implement a project whereby a developing country may produce a suitable package for sharing technology with other developing countries with the aim of initiating experimental plasma research it is necessary to consider the cost effectiveness of the device to be chosen. Does it produce a rich variety of plasma phenomena? Does it require an expensive vacuum system? Can its power supplies, control electronics and basic diagnostics be packaged at reasonable cost? What physical mechanisms operate to make the chosen device perform better at lower packaging cost than other devices? Can we understand and model the design and performance of the device so that we may effectively do research on it? What are the areas of research and potential applications of the device?

From the point of view of the production of a plasma with conditions of density and temperature sufficient for plasma fusion studies at an affordable cost there is little doubt that the class of fast magnetic compression devices known generally as the pinch, including the linear z-pinch, the superfast pinch, the gas-puff pinch and the plasma focus offers the best potential. We have considered this class of device and found that the plasma focus is most cost effective having the same power supply, control electronics and basic diagnostic requirements as the simple z-pinch and a much cheaper vacuum system with only rotary pump requirement, yet producing more intense plasma phenomena including copious x-rays, relativistic electron beam (REB) and fusion neutrons, all in one small easily packaged facility. What is the physics behind this cost effectiveness?

3.2 Cost Effectiveness of Various Types of Pinches:

We first recall that the neutron yield Y from a plasma fusion source is:

$$Y = \tfrac{1}{4}n^2 \langle\sigma v\rangle \quad \text{(volume)(time)} \qquad (27)$$

We note that Y is proportional to the square of n, the number density of the fusion fuel. We also note that starting from temperatures below 1 keV as one struggles to heat a plasma up towards a few keV, the effective cross section $\langle\sigma v\rangle$ for a thermalised deuterium plasma rises very rapidly with fuel temperature T. For example between 1 to 2 keV, $\langle\sigma v\rangle$ for the D-D fusion reaction goes up by a factor of 25! - and between 2 to 5 keV, another factor

of 30!. Thus the neutron yield is very sensitive to temperature. It is also proportional to the square of density.

In the pinch a large electric current is discharged from a capacitor bank through a gas between two electrodes. The current rises rapidly and due to the skin effect and wall conditions, electric breakdown first occurs across the glass wall of the container, forming a sheath of current along the glass wall. The electromagnetic $\underline{J}\times\underline{B}$ force in such a geometry acts radially inwards at every point of the current sheath so that, if the current is large enough, the current sheath and the heated gas (plasma) it entrains implode supersonically to form a hot dense column around the axis of the device.

The condition of balance between the hydrostatic pressure of the hot plasma and the constricting magnetic pressure gives the equation for the plasma temperature as:

$$T = \frac{\mu_o I^2}{8\pi N} \qquad (28)$$

where $N = \pi n r^2$ is the line density (particles m^{-1}) of the pinch. From this equation it would appear that since the temperature T depends on I^2 any temperature can be reached simply by increasing I to a sufficient value. However a pinch is essentially a dynamic device. The formation of the column has to occur in a time matched to the risetime of the current pulse, otherwise essentially the column is no longer there to obey the pressure balance equation when the current has risen to its peak value. Because of the dynamic nature of the problem the final temperature reached depends also on the implosion speed of the front of the plasma layer, which takes the form of a strong shock front. For deuterium the temperature dependence has the form:

$$T = 2.3 \times 10^{-5} \ (\text{shock speed})^2 \qquad (29)$$

Because of the dynamic nature of the problem it is essential for optimum use of the capacitor energy for the imploding shock wave to reach the axis at about the time of peak current. Now a typical well-designed capacitor bank for a pinch (say 20 kV, 60 μF, low inductance) has a current risetime of about 3 μs. In general it is difficult (and expensive) to design a capacitor bank of this conventional type for a much shorter risetime, and the bigger the bank capacity the longer tends to be the risetime.

So we consider a typical current risetime of 3 μs. A typical implosion speed cannot be much less than 10 cm/μs. At this speed the shock temperature in deuterium is 2×10^5 K, any slower and it is doubtful whether the magnetic 'piston' would be clearly formed. Even at this slow speed a radius of 30 cm for the pinch tube is required in order to match the current risetime. Now the imploding magnetic pressure is

$$P_m = \frac{\mu_o I^2}{8\pi^2 r^2} \qquad (30)$$

and with such a large pinch tube radius it is difficult to get enough magnetic pressure in the early stages of the implosion to start a clean compression unless the gas pressure is low. Thus a conventional pinch is limited by a (slow) current risetime of 3 μs, so that the pinch has to be operated with a large radius and hence low initial density. Moreover the speed (and hence temperature) becomes limited because of time-matching consideration.

What about the compressed density? Equation (26) gives us the following useful information:

(a) κ_m (and hence the compressed density ratio $\Gamma = \kappa_m^{-2}$) does not depend on the absolute magnitude of the current or the absolute length of the pinch.

(b) κ_m (hence Γ) depends on the time fuction of the current[5] and length.

(c) κ_m (hence Γ) depends on γ and f_{rs}. The smaller is γ, the smaller is κ_m and the larger is Γ[54]. As γ approaches the lower limiting value of 1, κ_m approaches zero and Γ tends to infinity. The larger is f_{rs}, the smaller is κ_m and the larger is Γ. The value of f_{rs} for a reflected shock on-axis, i.e. just after reflection is $f_{rs} = 4$ for cylindrical geometry[58]. As the reflected shock travels out from the axis we may expect f_{rs} to decrease towards a limiting value of 1.

For example for a constant current pinch with constant length, with $\gamma = 5/3$ and $f_{rs} = 1.6$, Eqn. (26) gives $\kappa_m = 0.301$ and hence a density compression ratio of $\Gamma = 11$. The corresponding figures for the deuterium plasma focus are estimated to be $\kappa_m = 0.14$ and $\Gamma = 50$. These values are independent of the magnitude of the plasma current. This limitation of the ability to compress is a serious one and implies that the performance of the pinch as a radiation source depends on its initial density.

There are several concepts to overcome this limitation. The gas-embedded axis-initiated z-pinch uses a laser to start a pinch discharge on-axis thus obviating the problem of matching the electrical risetime to the pinch collapse time and allowing the formation of a very small radius pinch (sub mm radius) in a very dense plasma (initial density up to several atmospheres). The device is however plagued with problems of instability[38]. The hollow pinch uses a controlled gas jet to form a thin plasma sheath which is then pinched into a vacuum. Using argon, krypton or xenon, the sheath does not thicken very much during the implosion because these gases[54] are in the 'freely ionizing' regime with a γ value having a small value of the order of 1.1. Because of the short distance between the imploding shock front and the magnetic piston the reflected shock from the axis hits the piston after a much shorter distance than that compared with a conventional pinch. The value of f_{rs} is hence closer to 4 than in a conventional pinch with its thicker plasma sheath. Thus the hollow-pinch has a reduced κ_m and has been operated successfully in the heavier gases, particularly krypton and xenon, for the production of x-rays for x-ray lithography and microscopy. However from the technical point of view the hollow pinch requires the additional development of a rather precise gas valve system. It is also not known to operate well in deuterium, probably because the collapsing deuterium sheath thickens as its γ goes to 5/3 once the sheath reaches a speed of the order of 10 cm/μs.

Ultra high power pinches have also been operated with pulse forming lines to reduce current risetimes so that the pinch may be operated at smaller radius, hence higher density[38]. This high power approach adds more complex and expensive technology.

3.3 Cost Effective Feature of the Plasma Focus:

On the other hand the plasma focus uses a very simple principle to overcome the time mismatch. Essentially it allows a conventional (slow risetime of 3 μs or more) capacitor bank to drive a very fast pinch (typically 1 cm radius in 50 ns) at a sufficiently high density and a large current during the time of pinch. Thus at low cost plasma conditions may be achieved which are more intense than that produced even in high-cost pinches.

The plasma focus uses a conventional capacitor bank to drive a device which has two sections:- the first section is a coaxial electromagnetic shock tube whose length is matched to the capacitor risetime. The rising capacitor current drives a shock wave axially down the shock tube at a suitable speed until the shock wave reaches the end of the tube at peak current. Then by the geometry of the device (see Fig. 4) the axial drive phase is simply converted to a radial compression or pinch phase.

The pinch phase is very intense (see Eqns. 28 and 30) because it starts at a very large current (typically 500 kA) and at a relatively small radius (typically 1 cm). Thus the operating pressure may be relatively high (10 torr in D_2 for a plasma focus against 0.1 torr or less for a pinch). The increased density and temperature more than compensates for the reduced volume in terms of the neutron yield Y as given in Eqn. (27).

Having seen from the basic physics mechanism that the plasma focus is capable of high levels of performance without special technological development the next step in the development of an educational package is to consider the modelling and design of a practical device.

3.4 Cost Effective Design of a Plasma Focus:

Design of the plasma focus may be based on the dynamic model, described in Chapter 2, which considers the focus dynamics in two separate phases - the axial run-down (shock tube) phase which crucially delays the radial focus, or pinch phase until the plasma current has reached its peak value (see Fig. 4). The first design point is therefore to have:

$$t_r = t_{a\,exp} \tag{31}$$

where

$$t_r = \frac{2\pi}{4} t_o \tag{32}$$

with

$$t_o = \sqrt{L_o C_o} \tag{33}$$

and

$$t_{a\,exp} \sim 2t_a \tag{34}$$

where

$$t_a = 2\pi \left[\frac{(c^2-1)}{\mu \ell n c}\right]^{\frac{1}{2}} \frac{z_o \rho_o^{\frac{1}{2}}}{(I_o/a)} \tag{35}$$

Equation (35) comes from the equation of motion of the axial phase and Eqn. (34) from an analysis of the trajectory.

Here t_r is the current risetime and $t_{a\ exp}$ is the transit time of the plasma layer for the axial phase. The quantities t_o and t_a are characteristic times of the axial phase according to the model. Here L_o is the inductance of the capacitor C_o together with all connections up to the plasma section of the focus tube, $c = b/a$, 'a' and 'b' are respectively the inner and outer radii of the focus tube, z_o its length, ρ_o the ambient gas density, μ the permeability of the plasma (same as the permeability of free space) and

$$I_o = V_o/(L_o/C_o)^{\frac{1}{2}} \tag{36}$$

where V_o is the initial voltage on the capacitor.

The second design point involves the characteristic 'pinching' time of the plasma focus phase. This may be shown from the equations of motion of the radial phase to be

$$t_p = \frac{4\pi}{\mu^{\frac{1}{2}}(\gamma+1)^{\frac{1}{2}}} a \frac{\rho_o^{\frac{1}{2}}}{(I_o/a)} \tag{37}$$

where γ is the specific heat ratio of the plasma. From this expression of t_p it is noted that the ratio of the characteristic axial transit time to characteristic focus time is

$$\frac{t_a}{t_p} = \frac{(\gamma+1)^{\frac{1}{2}}}{2} \frac{(c^2-1)^{\frac{1}{2}}}{(\ell nc)^{\frac{1}{2}}} F \tag{38}$$

where $F = z_o/a$.

A crucial factor in the operation of the Mathers plasma focus is that the axial phase occurs over a relatively long period $t_{a\ exp}$ enabling the build up of capacitor current. The pinch phase then occurs over a relatively short period t_p. During this time t_p approximately 10-20% of the initially stored energy is transferred to the pinch plasma in approximately 2% of the current risetime. This results in a power enhancement factor during the pinching phase which is crucial to the operation of the plasma focus. It is important then that the ratio t_a/t_p be of the order of 30 - 50 for the Mathers focus. Incidentally this results in a ratio of radial speed to axial speed of 2.5 for almost all plasma focus machines, large or small.

The third point to be considered in the design is that there are limits[56] of speed and pressure in the operation of the plasma focus. In deuterium for good focussing and consistent neutron yield, the axial speed just before focussing should be between the limits 6-10 cm/μs; the lower limit being the minimum speed required for a good snowplowing action in the axial phase and the higher limit being imposed by restriking of the discharge at the backwall or in the shock tube section. The limits of test gas pressure appears to be between 0.5 torr to 20 torr for deuterium; the lower limit apparently governed by re-striking; the upper limit by current filamentation.

The design of a plasma focus may take as a starting point the availability, or choice, of a capacitor bank. For the present exercise from the point of view of economy and cost-effectiveness a single Maxwell capacitor rated at $C_o = 30$ μF, $V_o = 15$ kV with an equivalent series inductance, ESL, of less than 40 nH was selected. A parallel-plate geometry was selected for the capacitor connections and the switch, with coaxial cables being used to connect the plasma focus input flanges. The value of L_o was estimated at 110 nH. Having fixed C_o and L_o Eqns. (33) and (32) give a value of t_r of 2.9 μs. Eqn. (36) yields $I_o = 248$ kA. The time matching condition of Eqn. (31) fixes $t_{a\ exp}$ at 2.9 μs. The value of z_o was then chosen at 16 cm to give an average axial speed of 5.5 cm/μs or a peak axial speed[10] of ∿9 cm/μs just before the focus phase. This axial speed is expected to be suitable for a good focussing action in deuterium.

The value of I_o is considerably smaller than most operational plasma focus machines which typically have I_o of the order of 500 kA or more. Observing from Eqn. (35) that the axial speed is $\sim I_o/(a(c^2-1)^{\frac{1}{2}}\rho_o^{\frac{1}{2}})$ and from Eqn. (37) that the radial speed is $\sim I_o/(a\cdot\rho_o^{\frac{1}{2}})$ it is noted that a reduction in I_o may be compensated in the first instance by a reduction in 'a' in order to maintain the axial speed within the speed limit indicated earlier. Thus we design for a = 9.5 mm and b = 32 mm which are smaller than typical values of most operational plasma focus devices. Moreover the value of $\frac{b}{a} \sim 3.4$, in this case, is near optimum. It is also noted that the value $t_a/t_p = 40$ for this design.

Having fixed the values of I_o, z_o, b and a and t_r it remains to fix the value of ρ_o from Eqn. (35). This gives $\rho_o = 0.21 \times 10^{-3}$ kgm^{-3}. This is the density of deuterium at 0.9 torr, which is within the pressure limits for deuterium focus operation as mentioned earlier.

The above design parameters have been subjected to a computation using the dynamic model in which the axial trajectory is computed using a snowplow model and the radial dynamics is traced using a generalized slug-model which considers the pinching plasma of increasing length with the plasma layer lying between a shock front at position r_s and magnetic piston at position r_p (see Fig. 4). This model has the advantage of giving a realistic final pinch radius ratio. Using the design parameters for the present device, the scaling parameters for the generalized slug model are:

$$\alpha = \frac{t_o}{t_a} = 1.26, \qquad \text{and } \beta = \frac{L_a}{L_o} = 0.36 ,$$

where L_a = maximum inductance of axial phase = $z_o(\mu/2\pi)\ell nc$. Also

$$\alpha_1 = \frac{t_a}{t_p} = 40.0 , \quad \text{and } \beta_1 = \frac{\beta}{\ell nc} = 0.294 .$$

The other parameters used for the model are c = 3.37, F = 16.84 and γ = 5/3 (for fully ionized deuterium).

The computation indicates a strong focus with a large focussing voltage spike. The parameter α was varied between 0.7 to 1.5 (corresponding to pressure range of 0.5 torr to 2 torr) and the computation repeated at each α. Good focussing was indicated over this range of pressure. These computation results add confidence to the design of the plasma focus. However it has been found that machine effects such as current and mass shedding[56], reduced channel size due to boundary effects and current re-strike which are not included in the dynamic model may alter the actual performance of the plasma focus. It is therefore to be expected that in actual operation the focus may need to be tuned by a variation of the five parameters V_o, ρ_o, z_o, a and b. If the design is not too far from optimum, operation over a range of ρ_o may be sufficient to establish a regime of good focus.

3.5 Scaling of Neutron Yield:

Experimental data on neutron yield have indicated a scaling law for neutron yield per pulse Y as a function of capacitor energy E. This scaling law (for operation in deuterium) may be written approximately as:

$$Y = 10\ E^2 \qquad (39)$$

where E is in joules; and appears to be approximately followed over the whole range of energy over which data is available i.e. 1 kJ to 1 MJ.

This scaling law may only be used with care since this scaling must depend on how efficiently the energy is coupled into the focus region. In other words, 2 devices having the same storage energy could be expected to have quite different yields unless they have been optimised within similar ranges of parameters such as external inductance and capacitor voltage.

A similar scaling law with tube current has been deduced from experimental data as:

$$Y \sim I^{3.3} \qquad (40)$$

This rule has to be used even more carefully for several reasons. The first reason is that for the two scaling laws to be both true implies that those devices whose data contribute to the deduction of the laws must have been operated with a fixed relationshop between E and I. Secondly the neutron production should probably be scaled to the focus current rather than the tube current, as it is known that these two currents are not the same and it has not been proven that the focus current is always a fixed fraction of the tube current for all devices.

However this does not mean that the scaling laws have no use. Most capacitors used for focus work are in the voltage range of 20 - 40 kV and are connected so that the total bank (stray) inductance is in the region of 20 - 40 nH. The ratio b/a is in the range 2 - 3.5 and with a capacitance of 20 - 100 μF, most of these devices can be similarly optimised so that corresponding to an energy of 1 kJ one can expect reliable neutron production $N \sim 10^7$ per pulse. In the other extreme of 1 MJ neutron pulse $\sim 10^{13}$ can be expected. An $n\tau$ scaling has recently also been suggested[48].

CHAPTER 4

SUB-SYSTEMS OF THE PLASMA FOCUS EXPERIMENT

The emphasis of this discussion will be on the design and construction of a simple, fully operational device. The first step in the planning of a focus experiment is probably in the assessment of the capacitor bank characteristics.

4.1 Capacitor Bank:

Firstly the operating voltage. There is a lower limit to the operating voltage given by the inductive voltage drop across the focus tube during the axial acceleration phase. This is estimated from (d/dt)(LI) where L, here, is the tube inductance. We take the approximation that

$$\frac{d}{dt}(LI) \sim I \frac{dL}{dt} \qquad (41)$$

since for the part of the acceleration period when this voltage is greatest, the current would have risen to large values so that the term L dI/dt is small compared to I dL/dt.

With $L = \frac{\mu}{2\pi}(\ell n \frac{b}{a})z$, we have

$$I \frac{dL}{dt} = I \frac{\mu}{2\pi}(\ell n \frac{b}{a}) \frac{dz}{dt} \qquad (42)$$

Typically with $\ell n \frac{b}{a} \sim 1$ and $I \sim 2 \times 10^5$ A, this gives an inductance voltage of 0.4 kV per unit axial speed of 10^4 m/sec (1 cm/μs). The range of suitable axial speeds in a plasma focus tube has been found to be rather small. The lower limit is fixed by the requirement for the electromagnetic mechanism to operate with sufficient efficiency. This is generally taken to be in the region of 3 - 4 cm/μs in deuterium, corresponding to a shock temperature of 20,000°K - 30,000°K. One cannot hope to reduce the speed further to, say, 1 cm/μs since $T_2 \sim v_s^2$ and the full-ionization electrical conductivity $\sigma \sim v_s^3$ and at 1 cm/μs the temperature is a mere 2000°K with certainly insufficient ionization (consequently electrical conductivity) for the electromagnetic drive to be operative.

On the other hand experimental observations also show that it is difficult to obtain consistent focussing action when the axial speed approaches or exceeds 10 cm/μs because of current spoke formation. The range of acceptable axial speeds would appear to be between 8 - 10 cm/μs.

Thus from Eqn. (42) the inductive tube voltage is in the range of 3 - 4 kV for a small plasma focus. The capacitor bank driving this back emf should therefore have an initial voltage several times this. We have chosen for cost effectiveness a Maxwell fast discharge capacitor rated 15 kV 30 μF, hence with maximum energy storage of 3.3 kJ. The equivalent series inductance of this capacitor is rated at less than 40 nH.

Connections between elements of the bank must be of low inductance. These may be by means of wide parallel plates clamped close together with insulating films of mylar sandwiched by outer layers of polyethene.

For ease of connection between the parallel plate output of the capacitor bank to the coaxial input of the focus tube short coaxial cables may be used. By using a sufficiently large number of these cables in parallel, the inductance may be suitably reduced.

The life expectancy of this Maxwell capacitor operating at full voltage, 80% voltage reversal with 3 μs risetime is estimated, from Manufacturers derating curves, to be 50,000 discharges. For research usage this should give a life expectancy in excess of 10 years.

4.2 Spark-gap Switch and Triggering Electronics:

A simple parallel-plate spark gap with a swinging cascade configuration (see Fig. 15) was developed giving a low inductance at minimum cost. The ratio of the gap is 3:2 (4½-3 mm). The gap is triggered via an isolating capacitor from an 800-V SCR unit via a TV transformer that was found to have a step-up ratio of 50 times and a risetime of 1 μs. The isolating capacitor is a 1 m length if UR67 coaxial cable. The parallel-plate spark gap is made from ½-in. thick copper plates and proved maintenance free for 200 discharges between 13-15 kV before it was cleaned. The triggering jitter was found to be within ± 50 ns. The circuit is shown in Fig. 15a. The SCR trigger circuit is shown in Fig. 15b.

The arrangement for the capacitor, the connecting plates, the spark gap and the output coaxial cables is shown in Fig. 16a. To keep the inductance low, the Earth plate of the capacitor (labeled no. 10) is extended nearly up to the anode and insulation is provided by a nylon cap (no. 5) around the anode stud. The cap dips into a pool of oil (no. 4) that is prevented from splashing out by means of an O-ring (no. 8). Mylar

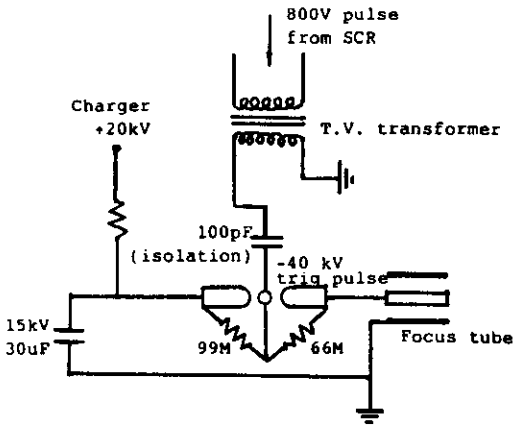

Fig. 15a Circuit for the swinging-cascade spark gap and focus tube.

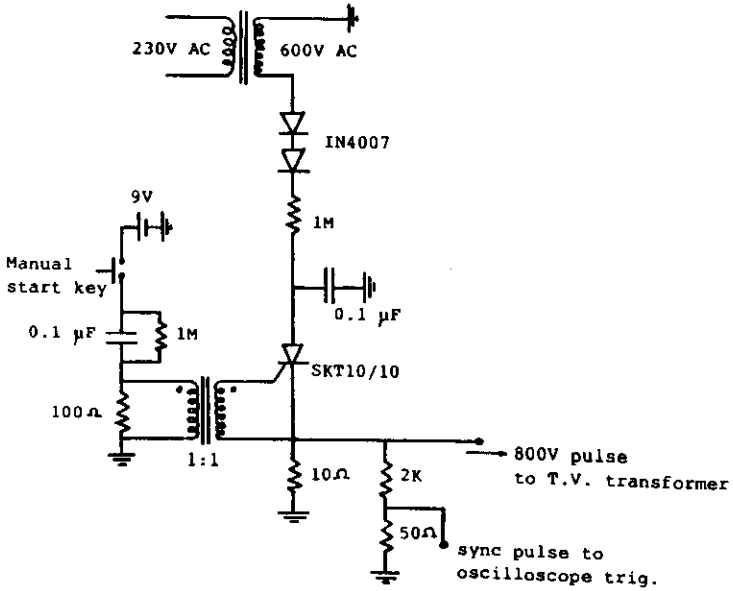

Fig. 15b Trigger and synchronizing electronics.

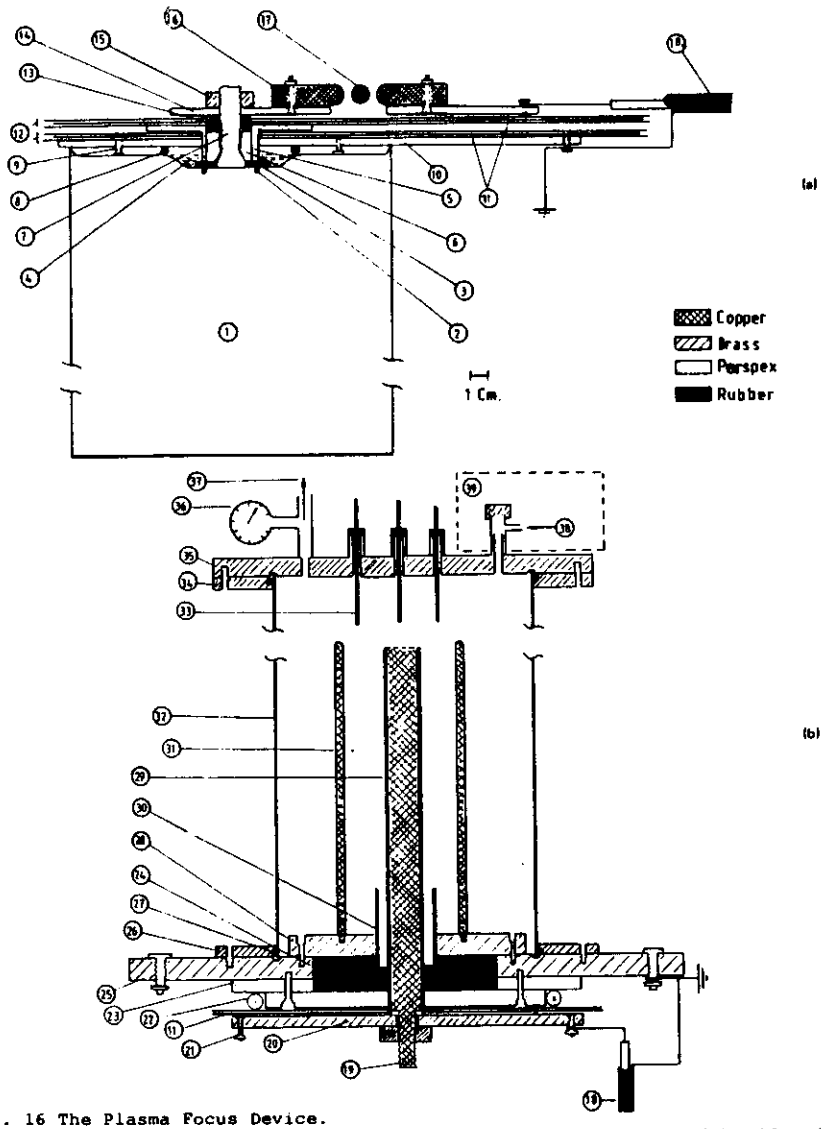

Fig. 16 The Plasma Focus Device.

(a) The capacitor connecting plates, the spark gap, and output coaxial cables. 1 = 15-kV, 30-μF capacitor; 2 = capacitor O-ring seal; 3 = washer; 4 = oil; 5 = nylon cap; 6 = steel nut; 7 = capacitor output seal; 8 = O-ring seal; 9 = Earth stud; 10 = Earth plate; 11 = 5-mil Mylar film; 12 = polyethelene film; 13 = copper ring HV connector; 14 = capacitor high-voltage (HV) output plates; 15 = lock nut for HV plate; 16 = HV electrode for swinging cascade spark gap; 17 = trigger electrode; and 18 = output coaxial cables (16 in parallel). (b) The plasma focus tube. 18 = input coaxial cables (16 in parallel); 19 = stud of anode; 20 = anode collector plate; 21 = connecting points for coaxial cable HV lead; 22 = Rogowski coil; 23 = perspex spacer; 24 = rubber holder; 25 = cathode collector plate; 26 = mild steel flange; 27 = O-ring seal; 28 = focus cathode support plates; 29 = focus anode; 30 = glass insulator; 31 = focus cathode (6 rods); 32 = mild steel focus chamber; 33 = movable magnetic probe in glass jacket; 34 = flange; 35 = back flange; 36 = diaphragm gauge; 37 = outlet to vacuum pump; 38 = inlet for test gas; 39 = wax container with indium foil and PM-scintillator activation counter.

sheets (no. 11), 2 in. wider all around than the conducting plates, sandwiched by polyethylene sheets (no. 12) complete the insulation between the HV plate (no. 14) and the Earth plate as shown in Fig. 16a. The Earth plate (no. 10) runs unbroken to the output position where the Earths of the coaxial cables connect. On top of the insulating sheets the HV plate is connected to the spark gap. Between the spark gap electrodes and all along it is placed a ½-in. diameter copper tubing (no. 17) that acts as the trigger electrode. The output plate of the spark gap is connected to the focus tube by means of 16 coaxial cables (no. 18) used in parallel.

4.3 The Plasma Focus Tube:

Essential to the structure of the focus tube is the backwall (see Fig. 16b) insulator. The glass insulator (no. 30) plays an important role in the symmetrical formation of the current sheet and has to be properly mounted to avoid being broken by vibrations. In the present design this glass insulator is mounted in a rubber holder (no. 24) which when compressed tightly and symmetrically by the brass flange (no. 28) grips the glass insulator. The rubber holder also acts as a vacuum and high-voltage seal. Figure 16b also shows the anode collector plate (no. 20) and the cathode collector plates (no. 25) onto which the coaxial cables connect.

The plasma chamber (no. 32) consists of a 30 cm length of 6½-in. diameter mild steel tubing that is chromed. Vacuum is provided by a single-stage rotary pump reaching an ultimate base pressure ~0.01 torr. The system was adjusted for a leakage rate of less than 2 μ/min and pressure is read with a mechanical diaphragm gauge. Operating at a test pressure of 1 torr and with a delay of less than 5 min between gas filling and focus operation, the air impurity in the system is about 2%. This level of vacuum proved to be sufficient for operating with good focus in various gases and good neutron yield when operated in deuterium.

4.4 Some Simple Diagnostics:

To measure the relative strength of the plasma focus action, a Rogowski coil (no. 22) with an integration time constant of 200 μs displayed on a 50 MHz CRO is used to measure the current flowing into the anode. A resistive voltage divider (not shown in figure) with 15 ns response time is strapped across the anode collector plate (no. 20) and the cathode collector plate (no. 25) to measure the voltage across the focus tube. In a plasma focus device, the axial drive phase is characterized by a smooth near-

sinusoidal rising current and a corresponding smooth waveform with a voltage value[56] that is proportional to the axial drive speed as the rate of change of current reduces to zero at peak current. As the focus occurs, the strong electromechanical action draws energy from the magnetic field pumping the energy into the compressing plasma. This mechanism is indicated in the distinctive current dip and voltage spike displayed by the current and voltage waveforms. In general, the stronger the focus, the more severely the plasma is compressed and the bigger the current and voltage spike.

To measure the magnetic field a 10-turn 1 mm coil jacketed in a 3 mm glass tubing (no. 33) is inserted into the focus tube and orientated to measure the azimuthal magnetic field. The passage of the current sheath driving the plasma layer may be measured as a sharp rise in magnetic field as the sheath sweeps past the probe. This measurement may be used to confirm the dynamics required to ensure a good focus.

An indium foil activation system is used to count fusion neutrons from the plasma. The system consists of an indium foil covering an NE 102 scintillator sittings on the photocathode of a 2-in. photomultiplier tube. The assembly is placed in a paraffin wax enclosure so as to thermalize the fusion neutrons. The detector is placed on the end flange of the plasma focus tube (no. 39). The PM tube is connected to a counter via a discriminator and a preamplifier and has a calibration constant of 5×10^4 neutrons per count, the counts being taken for a 30 seconds period immediately after the focus is fired.

4.5 Nitrogen Laser Shadowgraph System:

A very simple nitrogen laser system has been developed for pulsed plasma diagnostics using shadowgraphic, Schlieren or Mach Zehnder Optics[49].

The laser is excited by the conventional voltage swinging circuit schematically described in Fig. 17. The circuit theory of the parallel plate transmission line type of laser has been discussed in previous papers[60,61]. The two energy storage capacitors C_1 and C_2 of the circuit consist of a common earth plate, which is a 22 cm x 60 cm strip of kitchen aluminum kitchen foil laid on top of a flat aluminum plate (for electrical contact and mechanical support). Figure 18 shows the constructional details of the laser. On top of the foil are laid 3 sheets of 2 mil Mylar which extends at least 10 cm beyond the edges of the conductors all round. The high voltage plates of C_1 and C_2 are 22 cm x 40 cm and 22 cm x 17 cm strips

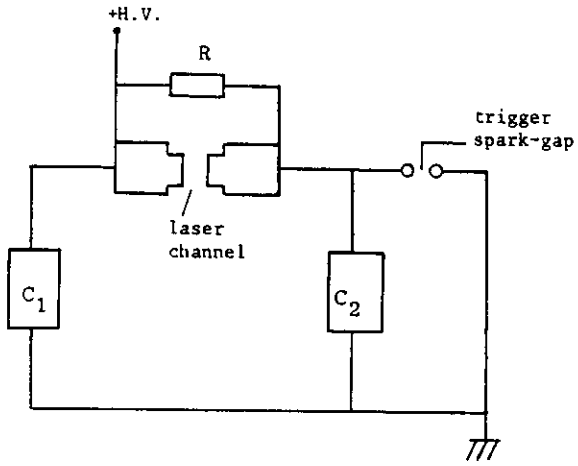

Fig. 17 Equivalent circuit of the nitrogen laser.

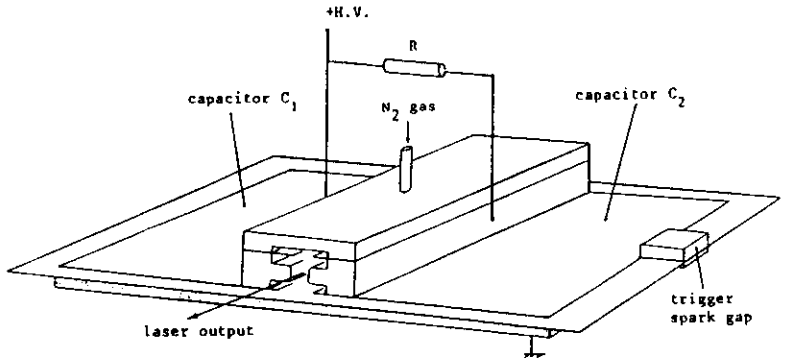

(a)

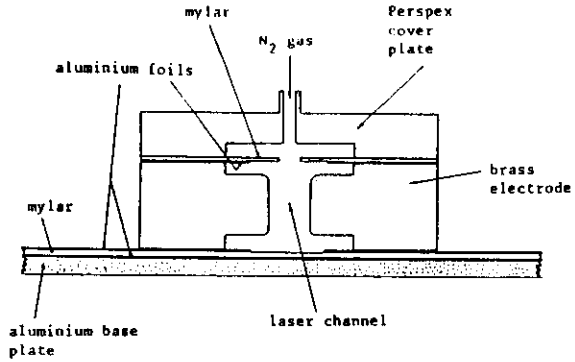

(b)

Fig. 18 (a) Sketch of a basic TEA nitrogen laser with Blumlein circuit.
(b) Cross-sectional view of the laser channel showing the preionizer system using aluminium foil-Mylar combination. The Mylar strips improve the preionization effect. (Ref. 49,50).

of aluminum foil laid on top of the mylar sheets. The measured values of C_1 and C_2 are 15 and 6 nF, respectively. On top of the foils are placed glass plates (6 mm thick) of approximate dimensions to prevent mechanical flexing of the foils during charging and discharging of the capacitors. The capacitor C_2 is mounted to a swinging cascade triggered spark gap. These high voltage capacitor plates are separated by a gap over which the laser channel is placed so that each side of the channel makes pressure contact with one of the capacitors. The electrodes of the laser channel are made of 20 cm long brass strips with cross-sectional dimensions of 0.5 in x 1 in and shaped as shown in Fig. 18b. The perspex plate is screwed onto the laser electrodes on the upper side over the top. Admission and evacuation of the nitrogen gas at atmospheric pressure is made through the middle and the ends of the channel, respectively.

In the arrangement shown, the edges of the high voltage capacitor plates (aluminum foils) are allowed to protrude beyond the edges of the laser electrodes into the laser cavity to act as corona blades for preionization. These form the set of blades on the lower side of the laser channel. A similar set of corona blades is placed on the upper side of the laser channel. The laser channel gap is set to 3 mm while the blades separation is typically set to about 40 percent greater than that of the main gap. The edges of the foils function as auxiliary corona electrodes which provide an initial distributed corona discharge to photoionize and prepare the laser channel for glow formation. The low-energy surface discharges acting as preionizing UV radiation sources are formed early during the rise of the voltage pulse across the laser gap and are distributed by corona charging of the Mylar surfaces that extend beyond the edges of the foils.

Optimum energy is obtained at a gap separation of 3 mm with a value of 300 μJ at 15 kV. The laser pulse duration is 1 ns with good beam quality.

The 1 ns pulse width of the nitrogen laser is sufficiently short to provide a freezing of motion of the order of 0.2 mm at a speed of 20 cm/μs.

The laser shadowgraphic set-up is as shown in Fig. 19. The laser pulse is correctly timed to catch the plasma focus at any time during the axial or radial phase by using variable delay units linking the plasma focus triggering pulse to the laser triggering pulse.

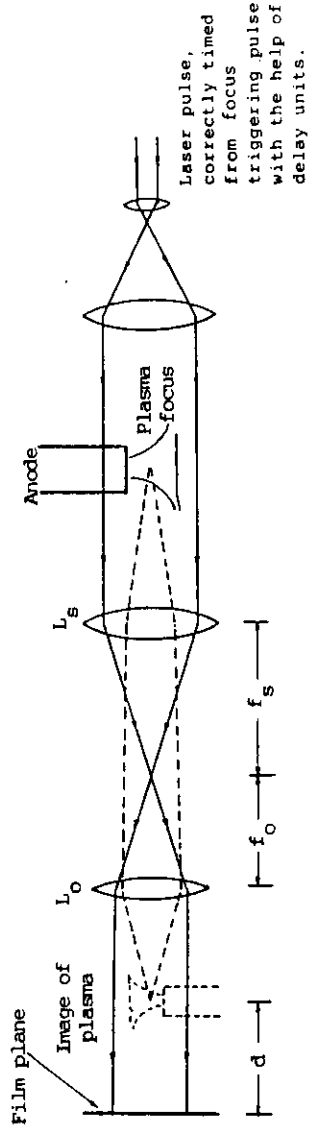

Fig. 19 Optical layout of the shadowgraph system. The plasma focus chamber, window and interference filter are not shown. (Ref. 50).

4.6 High Voltage Charger:

We may consider the question of power supplies for charging the capacitors. The alternative to buying costly power supplies is simply to build them. For example to charge a 15 kV 30 μF capacitor bank a power supply may be build up of the following components:

i) a transformer with an output rating of 15 kV RMS, 50 mA.

ii) 50 pieces of the commonly available IN4007 diodes, each the size of a grain of rise, rated at 1 kV blocking voltage, 1 A current.

iii) Connect these diodes in series and insert into a plastic hose (garden hose variety will do) filled with transformer oil. Design connectors to fit the ends of the plastic hose so that the ends of the diode chain protrude out, one at each end, whilst keeping the oil in.

Connect one end of the transformer to the positive side of the capacitor via the diode chain (observe polarity) in series with a suitable current-limiting resistor. Connect the other end of the transformer to the earth side of the capacitor. The simple half-wave rectifier system will quite satisfactorily perform its duty fo charging up the capacitors, especially if some care is taken to avoid sharp points at the connections exposed to air.

The design of the charger must incorporate a feature to dump the capacitor bank to ground through a ballast resistor in the event of power failure. Also a word of warning must be heeded about the high voltage of such a charger and the capacitor bank. These two pieces of equipment are definitely lethal and sufficient care must be given to the safety procedure to be observed in the design and operation of such equipment.

A more efficient way to build a charger is to use switching methods so that the voltage transformation may be done at frequencies higher than the mains frequency. This would involve the use of more efficient, weight-effective, cost-effective ferrite cores. For example for the nitrogen laser charger the EHT power supply of a television set may be used. A simple adaptation from such a set results in a 2 kg palm-sized 25 kV (variable) power supply with 1 mA current which is ample for the nitrogen laser.

CHAPTER 5

SOME RESULTS AND APPLICATIONS

5.1 Results:

The system was tested between 13 and 15 kV in various gases including air, argon, hydrogen and deuterium. The strength of the focusing action is gauged from the current dip and voltage spike. Figure 20a shows an oscillogram of the current and voltage waveforms of the plasma focus in 0.5 torr of air, with focusing action about 1 μs after peak current. Figure 20b shows a deuterium focus, at 13 kV, 2.5 torr with focusing action occurring at peak current. The deuterium focus shows signs of a secondary focus occurring some 0.4 μs after the first voltage spike. The occurrence of definite clean dynamics in the axial region preceding the focus region is confirmed by magnetic probe measurements. Figure 20c shows the output of a magnetic probe (lower trace) placed at $z = 10.2$ cm (i.e. in the axial drive region 10.2 cm from the backwall) in a discharge of 15 kV, 3.5 torr of deuterium. From this oscillogram and in comparison with the current oscillogram (upper trace) it is found that the current sheath arrives 0.6 μs before focusing occurs off the end of the anode at $z = 16$ cm giving a speed of 9.7 cm/μs (corresponding, from shock theory, to a temperature $\sim 2 \times 10^5$ K) over this section ($z = 10.2 - 16$ cm) of the axial drive region. From the risetime (10%-90%) of the magnetic signal and the speed this gives a current sheath thickness of 2 cm. The thickness and speed of this current sheath is typical of that in a good plasma focus system. The current dip during focusing is also seen as a dip in the magnetic probe output that shows two other current dips occurring at 0.2 and 0.6 μs after the dip. These confirm the occurrence of multiple focusing in deuterium in the device.

In air good focus was obtained at 13 and 15 kV in a narrow pressure range of 0.5-1.1 torr. In argon the pressure range for good focusing is greater at 0.3-3 torr. At 15 kV very strong focusing action was obtained at 0.8 torr. In helium the range of focusing is from 0.7 to 3.5 torr while in carbon dioxide focusing is observed below 1 torr. In hydrogen the pressure range for focusing is 1.1-6 torr. However, it is noticed that the focusing action, although definite, is not as intense, in terms of a focusing voltage spike, as in argon. The strongest focus

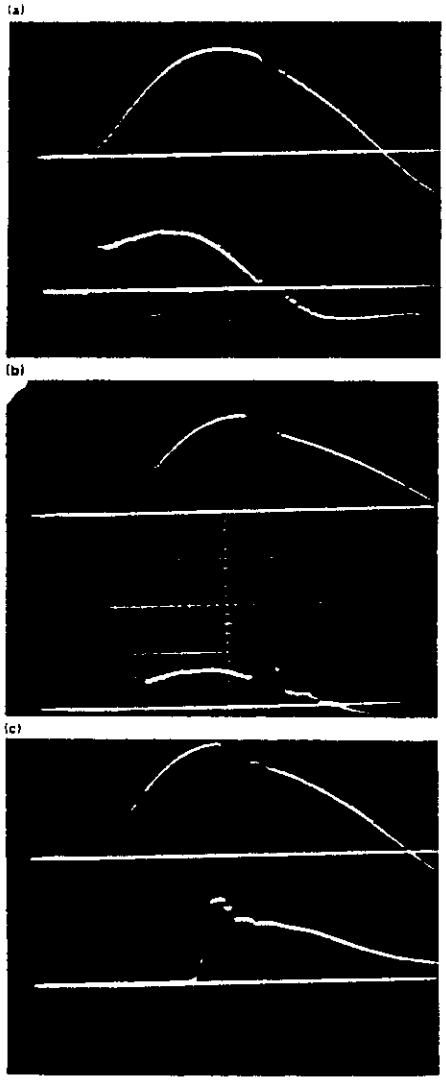

Fig. 20 (a) Current (upper trace) and voltage (lower trace) of plasma focus in air: 13 kV, 0.5 Torr; Top trace: 73 kA/cm; Bottom trace: 2 kV/cm; Time scale (horizontal): 1 μs/cm. (b) Current and voltage trace of plasma focus in deuterium: 13 kV, 2.5 Torr; Top trace: 75 kA/cm; Bottom trace: 4 kV/cm; Time scale (horizontal): 1 μs/cm. (c) Current and magnetic trace of plasma focus in deuterium: 15 kV, 3.5 Torr; Magnetic probe placed at z = 10.2 cm; Top trace: 73 kA/cm; Bottom trace: 0.6 T/cm.

in hydrogen occurs at 3.3–4.3 torr. In deuterium strong focus is observed at 1–5 torr with best focusing at 2.5–3 torr.

In deuterium when operated at 15 kV and optimum pressure conditions of 3 torr consistent counts of 1000–2000 are obtained using the PM-scintillator counter. This corresponds to 0.5×10^{8} neutrons per shot.

The system shows remarkably consistent and reproducible operation. Six systems were assembled one after the other and tested over a period of 2 months. Each system was assembled and tested over a period of 1 week averaging between 100–200 shots in the various gases. Once a system has been established to be operating normally, that is, without undue leakage and after an initial period of out-gasing involving some three to five discharges, proper focusing is achieved for better than 95% of the discharges, apart from those discharges deliberately operated outside the established suitable pressure range for the gas used.

5.2 Temperatures and Densities:

It is of interest to estimate the range of temperatures and densities available in this device. This is best discussed separately for each of the two phases of operation, namely, the axial drive phase and the radial collapse phase. In deuterium in typical operating conditions in the axial drive phase between $z = 8$ and $z = 16$ cm a steady plasma temperature of 2×10^{5} K may be estimated (Eqn. 29) in a 1-D slug length of 4 cm. For operating at an ambient density of 3 torr of deuterium, complete ionization is achieved at this temperature giving an ion density and an electron density each of about 10^{18} per cm^3 since a shock mass density ratio of 4 may be expected for a strong fully ionized deuterium shock. In the radial focus phase, soft x-ray techniques[5,40] have been used to estimate temperatures in a similar small plasma focus to be 0.7–3 keV while interferometric techniques[30] have been used to measure peak electron densities in the maximum compressed pinch column of $1–5 \times 10^{19}$ per cm^3. These experimental results agree with computations based on the dynamic theory already discussed.

When heavier gases such as argon are used as the test gas the dynamic theory predicts enhanced compression due to the specific heat ratio[22] being reduced below 5/3. In the case of argon, higher temperature (about 4 keV) and electron densities (10^{20} per cm^3), may then be predicted

by the dynamic theory applied to the pinch phase. There is also experimental evidence[23] to back up these predictions.

At such high temperatures, thermodynamic computations shows that even argon becomes almost fully ionized[54] and experimental work shows that worthwhile spectroscopic studies may be made of the focus using, e.g. argon as a test gas. Peacock[57] et al. have used a 2 m Rowland circle grating spectrograph and a de Broglie spectrometer to obtain spectrograms of argon and neon focus discharges. The results are sufficiently reproducible for identification of transitions in H-like and He-like Ne and Ar ions. If line profile scans are to be made then it is usual to obtain a profile over a number of discharges. The question of reproducibility then becomes important. In the present setup the reproducibility has been studied by using two simultaneous monitoring criteria. First, the neutron yield of each discharge is monitored and those that are beyond 10% of the average may be rejected. Second, the voltage spike is monitored for its time position and its shape (rate of rise, single spike, or multiple spikes). The time position of its peak (single peak spike) may be used as a reference point to fix the time position of the photomultiplier output. A discharge with a voltage spike shape that does not conform with the average shape may also be rejected. A close study of the data shows that when the system is properly set up and adjusted, at least 80% of the discharges are sufficiently reproducible for scanning applications.

5.3 Experiments and Applications:

It may also be of interest to inquire about the types of experiments that may be done on a plasma focus machine. First, as already mentioned in detail earlier, the axial drive phase may be used to study plasma dynamics and energetics[19]. The use of simple voltage, current and magnetic probes, together with a coupled circuit-dynamic analysis enables one to obtain the dynamics and energetics of the system and also shock plasma temperature and densities. These may be confirmed with spectroscopic and interferometric measurements to check the validity of the dynamic model used.

In the radial pinch phase, the pinching action is more severe than the Z or theta pinch for two reasons. The first is that the use of the axial drive phase delays the focus pinch so that it occurs at peak

current and enables a smaller radius pinch to occur at higher ambient density. Second, the smaller radius pinch is an elongating pinch that also contributes to an enhancement of pinch compression due to the smaller resulting pinch radius ratio[29]. Thus even a small plasma focus achieves sufficiently intense plasma conditions to produce consistent nuclear fusion and may be used as the lowest-cost device for demonstrating nuclear fusion from a plasma. Even a simple 3 kJ device such as the one presently discussed here may be used as a starting point for studying neutronics. For example, measurement of the half-life of ^{116}In has been carried out[58] using the UNU/ICTP PFF as the neutron source. It is known that the deuterium focus produces a deuteron beam[30] of several hundred keV. The effect of this beam on targets may also be studied for the enhancement of neutron yield. The corresponding electron beam, accelerated in the opposite direction into the anode, has relativistic speed and may be taken out of the system by using a hollow electrode. Thus the focus may also be used as a REB source. These two effects, i.e. consistent neutron and REB production, are not available in the Z pinch and theta pinch because of insufficient densities (10^{17} per cm^3) and temperatures (several hundred eV). This demonstrates the enhanced intensity of the plasma focus device.

The REB may also be used to sputter anode material downstream of the focus[30,59]. By using different materials as inserts in the anode face, different materials may be sputtered.

The question of neutron scaling is by no means closed. Lee[52] has shown that the observed neutron scaling of $Y \sim E^2$ and $Y \sim I^4$ is due to the speed limitation (10 cm/μs axial speed) and density limitation (about 20 torr) which has been observed for all plasma focus, small or large. If the focus could be operated with increased axial speed, say to 20 cm/μs, there are reasons to believe that the neutron yield would increase dramatically. Recent laser Schlieren photographs[49] (Fig. 21) have given some clues that the speed limitation may be due to current sheet - shock front decoupling at higher speeds associated with sheath inclination and a γ-effect. Further studies should be made to see if conditions may be adjusted to remove the speed limitation and hence improve the neutron scaling law.

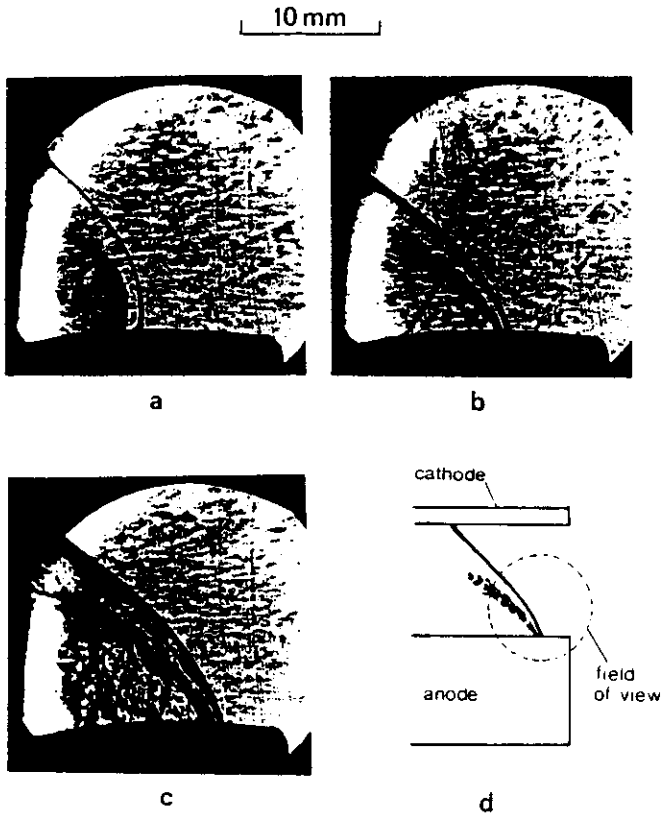

Fig. 21 Schlieren images of the plasma focus discharge in the axial rundown phase. The plasma focus device was operated at 14 kV and with deuterium gas at (a) 1 mbar, (b) 9 mbar, and (c) 14 mbar.

Other experiments and applications may be listed.

a) for studying a plasma under nuclear fusion conditions.
b) for developing diagnostics for fast pulsed plasmas.
c) as a neutron source for blanket studies for fusion reactors, pulsed neutron radiography, pulsed activation analysis, nuclear weapons simulation.
d) as an intense source for UV light, soft x-ray and electromagnetic radiation for spectroscopic applications, pump source for UV and soft x-ray laser, x-ray diagnostics and Electromangetic Pulse (EMP) studies.
e) for production of extreme magnetic fields and associated possibility of solid state compressions.
f) as a thermonuclear reactor; potential exists because of the observed $Y \sim E^2$ relationship.

In the experience of the UNU Training Programme the study of plasma dynamics particularly in the axial drive phase and the demonstration and study of plasma nuclear fusion are in themselves sufficiently interesting and of sufficient scope for a good beginning to be made in the field of experimental plasma physics.

REFERENCES

1. P.P. Petrov, N.V. Filippov, T.I. Filippova and V.A. Khrabrov in "Plasma Physics and the Problem of Controlled Thermonuclear Reactions" (Ed. M.A. Leontovich) Vol. IV pg. 198, Pergamon, New York (1960)
2. N.V. Filippov, T.I. Filippova and V.P. Vinogradov, Nucl. Fusion Supple. Pt. 2, 577 (1962)
3. N.V. Filippov and T.I. Filippova, Proc. of Second Conf. on Plasma Physics and Controlled Nucl. Fusion Research 1965, 2, IAEA (1966)
4. J.W. Mather, Phys. Fluids Supple., 7, 5 (1964)
5. J.W. Mather, Phys. Fluids, 8, 366 (1965)
6. J.W. Mather, Procs. of Second Conf. on Plasma Physics and Controlled Fusion Research 1965, 2, IAEA (1966)
7. E.H. Beckner, J. Appl. Phys., 37, 4944 (1966)
8. M.J. Bernstein, D.A. Meskan and H.L.L. van Paassen, Phys. Fluids, 12, 193 (1969)
9. C. Maissonnier, F. Cipolla, C. Gourlan, M. Haegi, J.G. Linhart, A. Robouch and M. Samuelli, Procs. 3rd Conf. on Plasma Phys. and Controlled Nucl. Fusion, Novosibirsk 1968, 2, IAEA Vienna (1969)
10. N.J. Peacock, Procs. 3rd Conf. on Plasma Phys. and Controlled Nucl. Fusion, Novosibirsk 1968, 2, IAEA Vienna (1969)
11. C. Patou, A. Simmonet, J.P. Watteau, Phys. Lett. A, 29, 1 (1969)
12. G. Decker, D.J. Mayhell, O.M. Friedrich, A.A. Dougal, Bull. Amer. Phys. Soc. (2), 13, 1543 (1968)
13. S. Lee, Y.H. Chen, S.P. Chow, B.C. Tan, H.H. Teh and S.P. Thong, Inter, J. Electronics, 33, 85 (1972)
14. S.P. Chow, S. Lee and B.C. Tan, J. Plasma Phys., 8, 21 (1972)
15. G.R. Hogg and J. Tendys, AAEC/E 280 (Australia) (1973)
16. M. Itoh, K. Hatori and K. Hirano, Jap. J. Appl. Phys., 13, 1033 (1974)
17. H. Conrads, D. Gollwitzer and H. Schmidt, Procs. 6th European Conf. on Controlled Fusion and Plasma Physics, Moscow, pg. 367 (1973)
18. L. Michel, K.H. Schoenbach and H. Fisher, Appl. Phys. Lett., 24, 57 (1974)
19. M. Gryzinski, A. Jerykiewicz and J. Nowikowski, Bull. de l'Academie Polonaise des Sciences techniques XXII, 2 (1974)
20. G. Decker, G. Pross, B. Rueckle, H. Schmidt and M. Shakhatre, Procs. 3rd Topical Conf. on pulsed high beta plasma, Culham (1975)
21. S. Lee and Y.H. Chen, Malaysian J. Science, 3B, 159 (1975)

22. J. Gratton, H. Kelly, M. Milanese, and J. Pouzo, Phys. Lett., A62, 422 (1977)
23. F. Gratton and J. Vargas, Procs. 7th European Conf. on Controlled Nucl. Fusion, Lausanne, I, 64 (1975)
24. S. Lee and T.H. Tan, Procs. 7th European Conf. on Controlled Nucl, Fusion, Lausanne, I, 65 (1975)
25. S. Sinman and A. Sinman, Fusion Energy - 1981 (ICTP, Trieste) IAEA-SMR-82, Vienna, pg. 327 (1982)
26. S. Lee, Fusion Energy - 1981 (ICTP, Trieste) IAEA-SMR-82, Vienna, pg. 289 (1982)
27. R. Gratton, C. Ferro Fontan, H. Kelly, J. Pouzo, M. Milanese, A. Sicardi Schifino, G. Lesin and M. Esper, Fusion Energy - 1981 (ICTP, Trieste), IAEA-SMR-82, Vienna, pg. 275 (1982)
28. S. Lee, Bul. Fiz. Mal., 3, 197 (1981)
29. S. Lee, Plasma Phys., 25, 571 (1983)
30 G. Decker and R. Wienecke, Procs. Twelfth Inter, Conf. on Phenomena in Ionized Gases, Eindhoven 1975, 2, 155 (1976)
31. Y.H. Chen "Parametric Study of Focus Optimization" Ph.D. Thesis, University of Malaya (1978)
32. S. Lee and Y.H. Chen, Procs. Twelfth Inter, Conf. on Phenomena in Ionized Gases, Eindhoven 1975, 1, 353 (1976)
33. S. Lee, Bul. Fiz. Mal., 2, 240 (1981)
34. D.E. Potter, Nucl. Fusion, 18, 813 (1978)
35. S. Lee, J. Appl. Phys., 54, 3603 (1983)
36. S. Lee and Y.H. Chin, Bul. Fiz. Mal., 2, 105 (1981)
37. S.P. Thong and S. Lee, Mal. J. Science, 2(B), 157 (1973)
38. M.G. Haines, Phil. Trans. Roy. Soc. Lond., A300, 649 (1981)
39. S. Lee, Y.H. Chen, S.P. Chow, B.C. Tan, H.H. Tah and S.P. Thong, Inter, J. Electronics, 33, 85 (1972)
40 S. Lee and Y.H. Chen, Fusion Energy - 1981 (ICTP, Trieste) IAEA-SMR-82 Vienna, pg. 297 (1982)
41. Y.H. Chen and S. Lee, Inter. J. Electronics, 35, 341 (1973)
42. C.S. Wong, S. Lee and S.P. Moo, Mal. J. Science, 6(B), 167 (1980)
43. S. Lee, J. Phys. D: Appl. Phys., 16, 2463 (1983)
44. D.E. Potter, Phys. Fluids, 14, 1911 (1971)
45. Reports of the IAEA Consultants' Meeting on IAEA Report (1978) Fusion Programme for Developing Countries.
46. T.Y. Tou and S. Lee, Bul. Fiz. Mal., 4, 189 (1983)
47. M. Sadowski, H. Herold, H. Schmidt and M. Shakhatre, Phys. Lett., 105A, 117 (1984)
48. H.J. Kaeppeler, A. Hayd, M. Maurer and P. Meinke, IPF-83-2. Institut für Plasmaforschung der Universitaet Stuttgart (1983)

49. K.H. Kwek, T.Y. Tou and S. Lee, J. Fiz. Mal., 9, 36 (1988); IEEE Trans. on Intrumentation and Measurement, IM-38, 103 (1989)

50. K.H. Kwek "Pinch Structure of a Plasma Focus", Ph.D. Thesis, University of Malaya (1989 - submitted)

51. S. Lee, T.Y. Tou, S.P. Moo, M.A. Eissa, A.V. Gholap, K.H. Kwek, S. Mulydrono, A.J. Smith, Suryadi, American J. Phys., 56, 62 (1988)

52. S. Lee "The sharing of fusion-related technology among developing countries" - invited paper read at the Energy Independence Conference, Rio de Janeiro, August 1987; Procs. "Fusion Energy and Plasma Physics" World Scientific, edited by P.H. Sakanaka, pg. 754 (1988)

53. Mohammad Zaka-ullah "A parametric study of the dense plasma focus" Ph.D. Thesis, Quaid-I-Azam University (1988)

54. S. Lee, Australian J. Phys., 36, 891 (1983)

55. G. von Guderley, Luftfahrtforschung, 19, 302 (1942)

56. "Laser and Plasma Technology", World Scientific, Ed. by S. Lee et al (1985)

57. N.J. Peacock et al., J. Phys. B 2, 798 (1969)

58. S.P. Moo and S. Lee, Singapore J. Phys., 4, 131 (1987)

59. S. Lee, Harith Ahmad, T.Y. Tou, K.H. Kwek and C.S. Wong, J. Fiz. Mal., 7, 1 (1986)

60. S. Lee, A.V. Gholap, A.J. Smith, K.H. Kwek, A.C. Chew, T.Y. Tou and S. Sapru, J. Fiz. Mal., 6, 165 (1985)

61. A.J. Smith, K.H. Kwek, T.Y. Tou, A.V. Gholap and S. Lee, IEEE J. Quan. Electronics QE-23, 283 (1987)

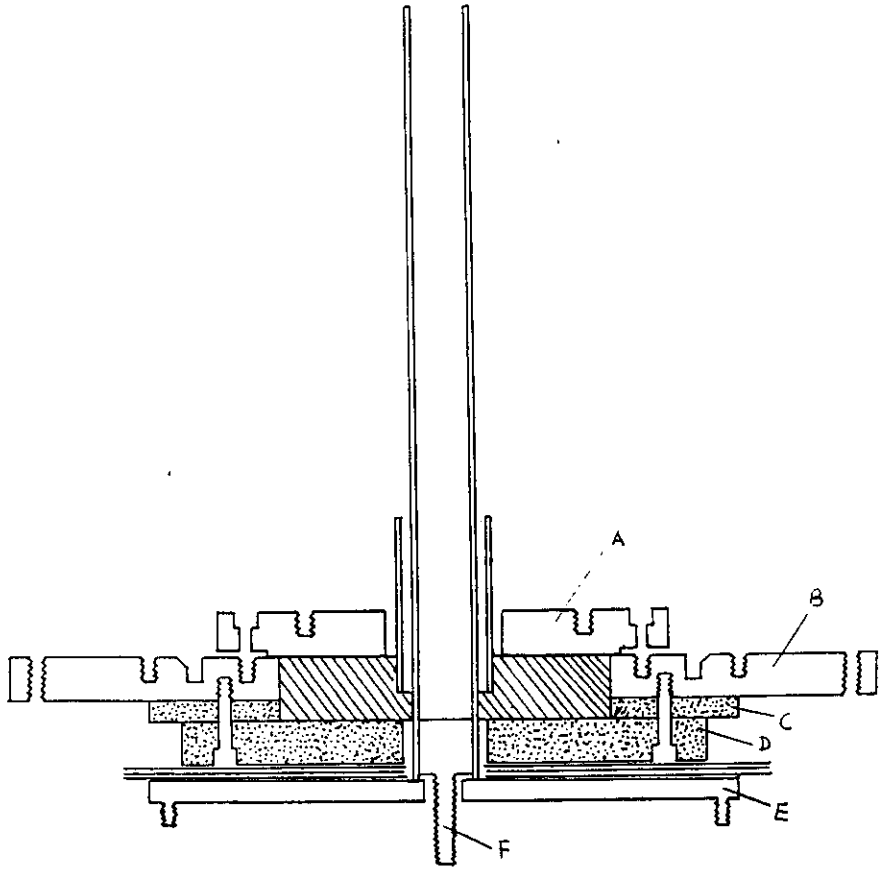

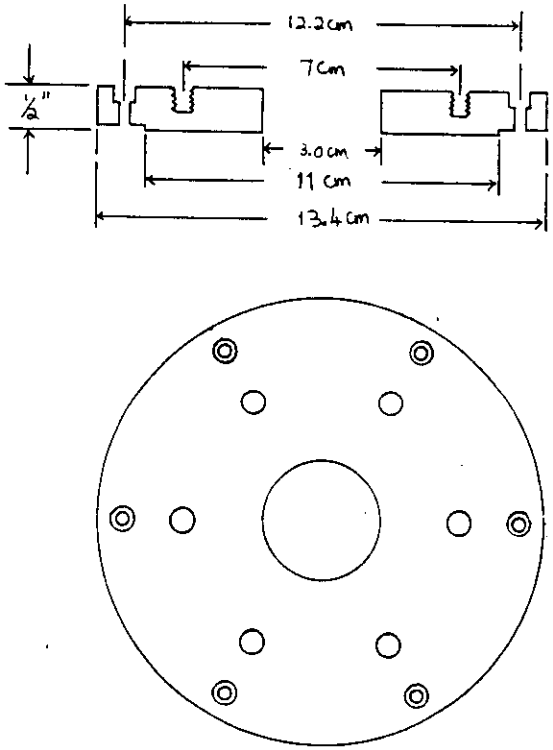
12.2cm
7cm
½"
3.0cm
11 cm
13.4cm

(B) Brass

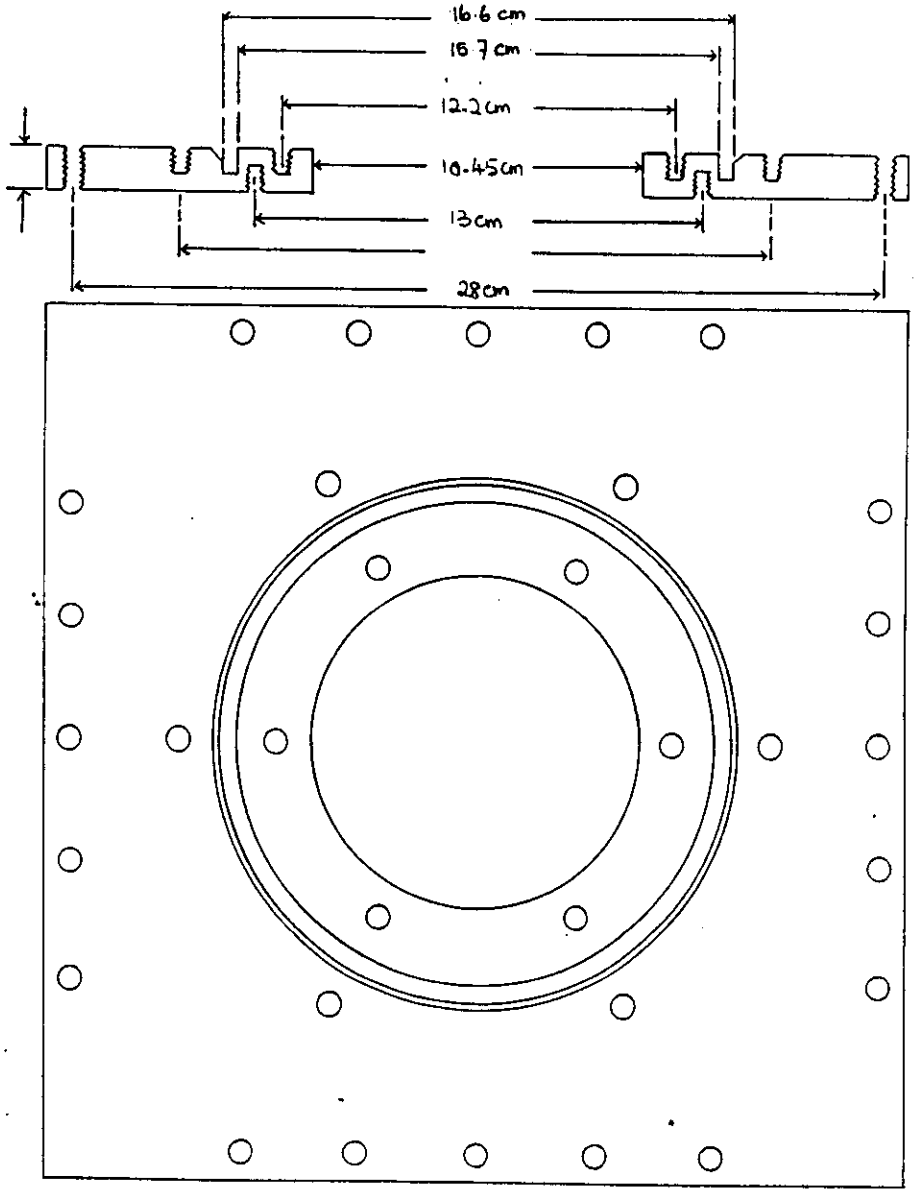
16.6 cm
16.7 cm
12.2cm
10.45cm
13cm
28cm

Perspex

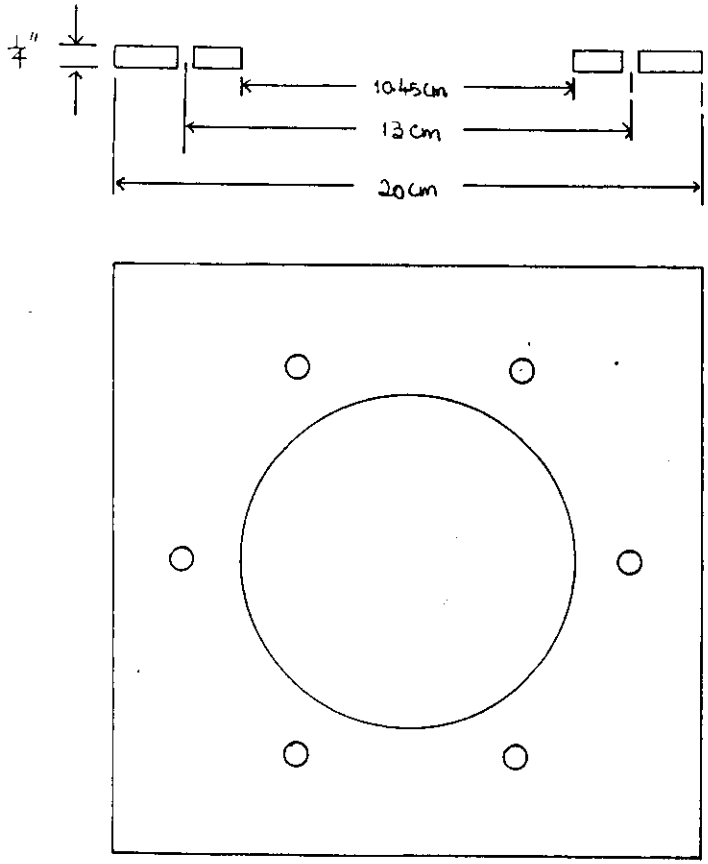

D) Perspex

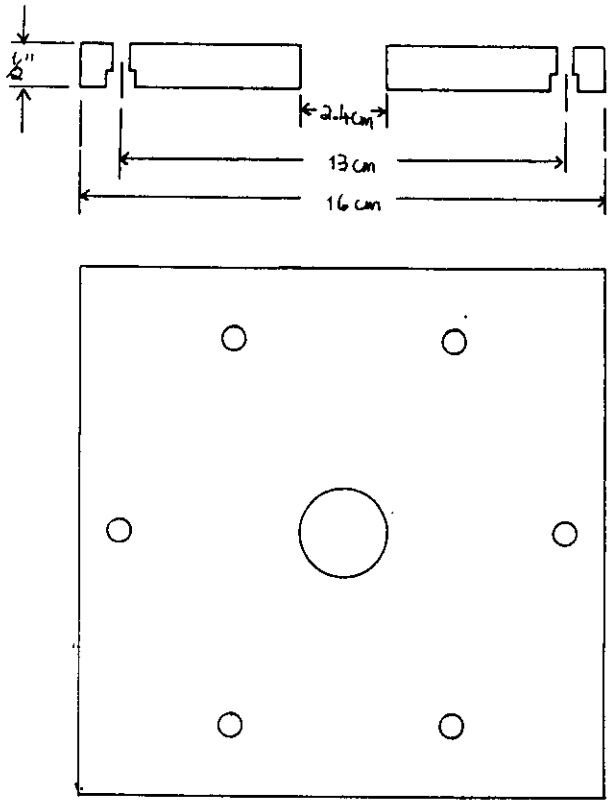

(E) Brass

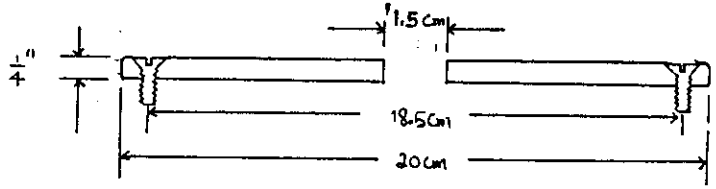

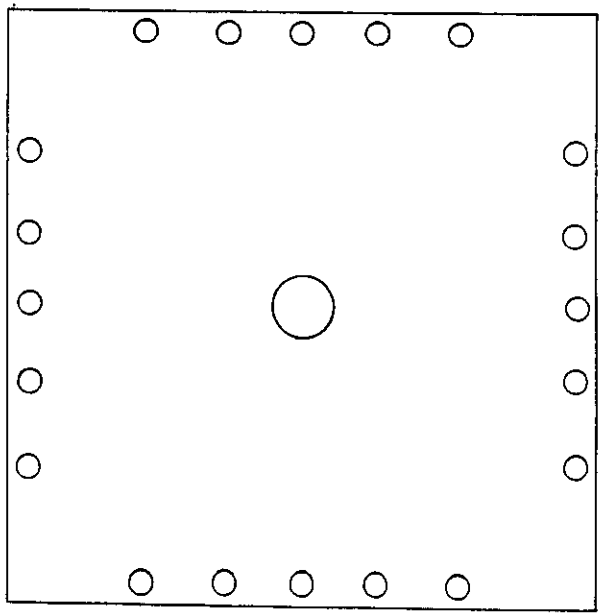

(F) Copper

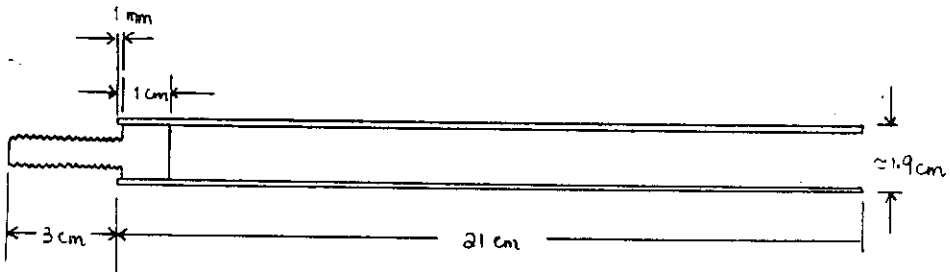

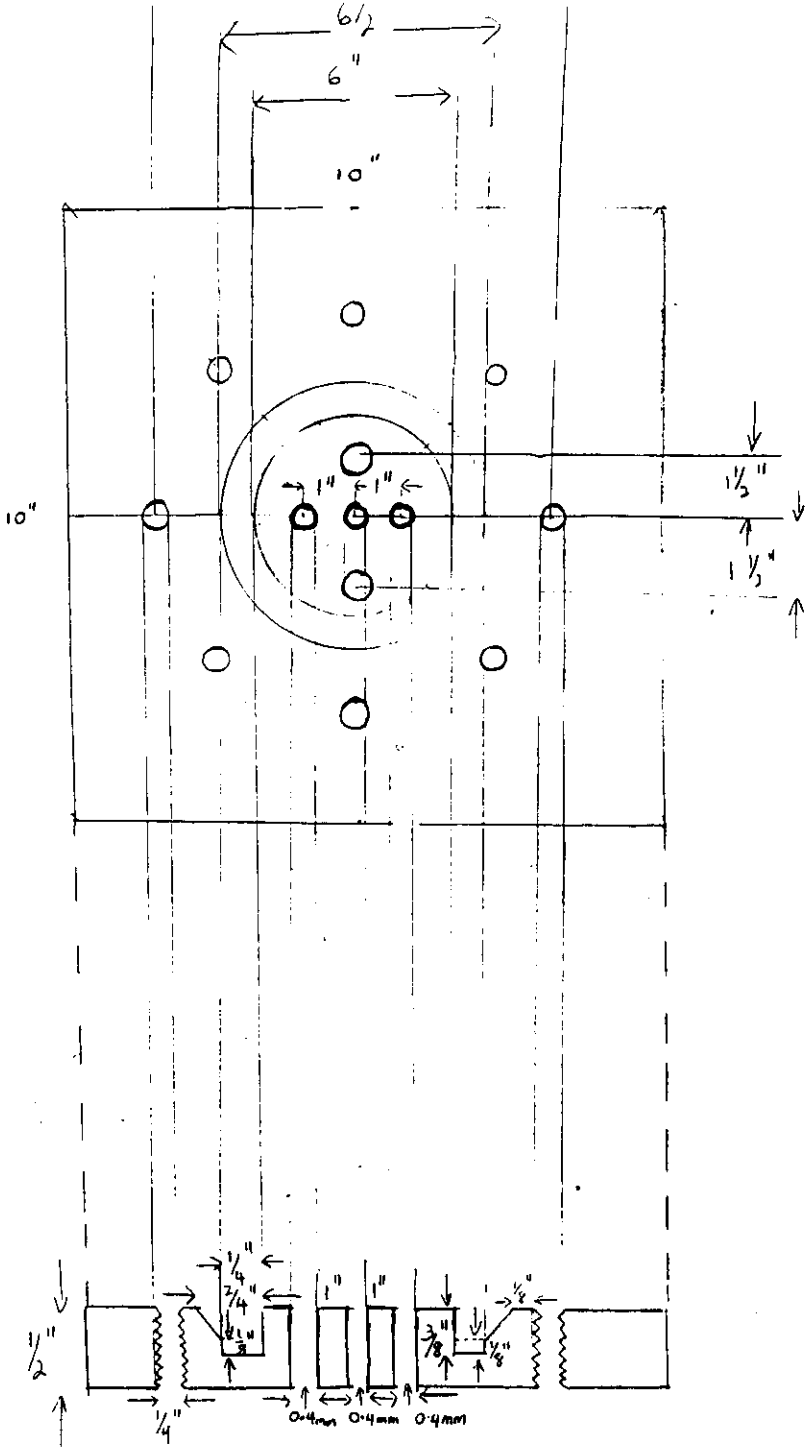
6½
6"
10"
10"
1"
1"
1⅓"
1⅓"
¼"
¾"
½"
⅜"
⅛"
½"
¼"
0·4mm
0·4mm
0·4mm

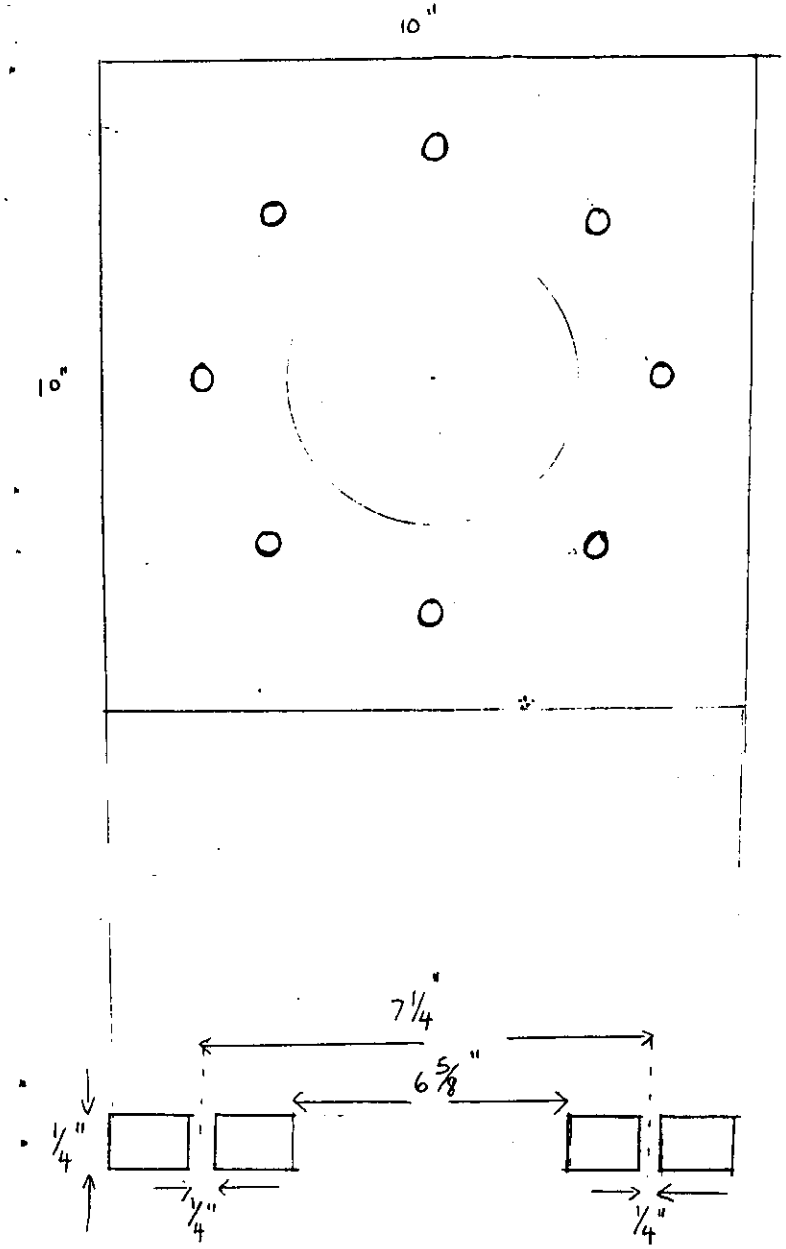
10"
10"
7¼"
6⅝"
¼"
¼"
¼"